Institute of Sensor and Actuator Systems

Piezoelectric Microsystems: Material Aspects, Devices and Applications

Donnerstag, 26. Oktober 2017

U. Schmid, M. Schneider

Univ.-Prof. Dr. Ulrich Schmid

- 1993-1998 Study of physics in Munich, Kassel, Nottingham (GB) and Frankfurt/Main
- 1998 Diploma thesis at the microelectronics research lab of the Daimler-Benz AG in Frankfurt/Main
  „Preparation and characterization of lateral field effect transistors in 6H-SiC“
- 1999-2001 Ph.D. student at the microsystem research lab of the DaimlerChrysler AG (EADS Deutschland GmbH) in Ottobrunn/Munich
- 2001-2003 Project leader at the EADS Deutschland GmbH in the field of advanced injection technologies
- 2003 Ph.D. degree of the TU Munich with a thesis entitled:
  „Robust flow sensor for high pressure automotive injection systems“
- 2003-2008 Post doc at the Chair of Micromechanics at Saarland University
- 10/2008 - Full professor for Microsystems Technology at the
- Vienna University of Technology
- 01/2012 - Head of Institute for Sensor and Actuator Systems

- Email Contact: ulrich.e366.schmid@tuwien.ac.at

Dr. Michael Schneider

- 2003-2009 Study of physics at Karlsruhe Institute of Technology (KIT)
- 2008-2009 Diploma thesis at Forschungszentrum Karlsruhe / KIT
  “Lorentzwinkel-Messungen an hochbestrahlten Silizium-Streifensensoren”
  „Lorentz angle measurements on highly irradiated silicon strip sensors“
- 2009-2014 Ph.D. student at the Institute of Sensor and Actuator Systems, TU Wien
- 02/2014 Ph.D. degree, TU Wien
  “Einfluss der Schichtdicke und der Substratvorbehandlung auf die elektromechanischen Eigenschaften von gesputterten Aluminiumnitrid-Dünnfilmen“
  „Impact of substrate thickness and pre-conditioning on the electromechanical properties of sputter-deposited aluminum nitride thin films“
- 03/2014 - Habilitant at the Institute of Sensor and Actuator Systems, TU Wien

- Email Contact: michael.schneider@tuwien.ac.at

8 Faculties, ~30.000 students

Electrical Engineering and Information Technology
Physics
Technical Chemistry
Informatics
Mathematics and Geoinformation
Civil Engineering
Mechanical and Industrial Engineering
Architecture and Planning

Electrical Engineering & Information Technology
2011: 10 institutes
(1st-year students: ca. 350)

Institute of Sensor and Actuator Systems

3 research groups:

- Micro- and Nanosensors (MNS)

S. Schmid, Keplinger

Opto-mechanical resonators, microfluidics, technology

- Applied Electronic Materials (AEM)

Nicolics

Packaging, thick film technology, ceramics

- Microsystems Technology (MST)

U. Schmid

MEMS, robust materials, technology

Currently circa 30 (state) + 25 (project funded)
(of which 20 PhD students)
+ ca. 10 undergraduate students

MEMS Technology

- Center for Micro- and Nanostructures (*ZMNS*)
- MEMS Technology Lab/Integrated Ceramic Technology

In total about 250 m^2 laboratory for sensor realization

Facilities include backside aligner, spray coater, wafer bonder.
Key equipment: DRIE,PECVD, LPCVD, electrochemical cell

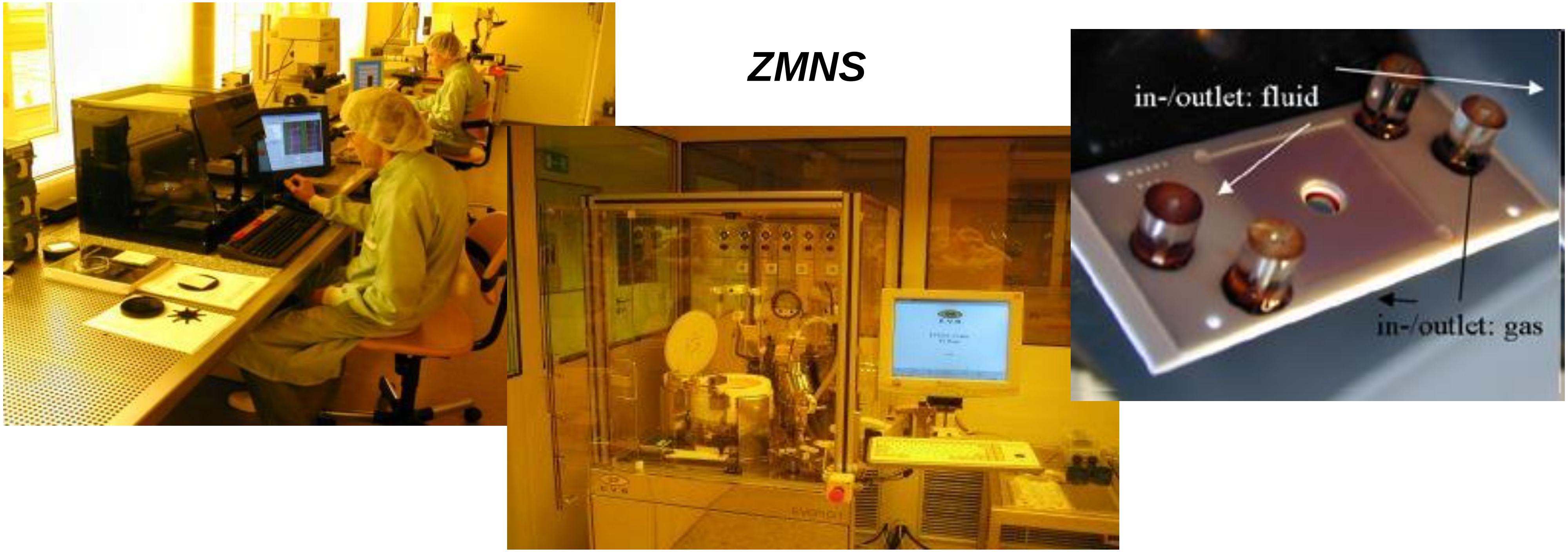

ZMNS

Research Group: Microsystems Technology

- **Expertise in the design, realization and evaluation of MEMS devices and systems**
- 2 Post-docs
- 13 Ph.D. students
- 3 research assistants
- 4 technicians
- 1 secretary
- 2 Ph.D. students (external)

- **Research topics**

- **Technology related activities:**
- Functional thin films (AlN, SiC)
- Robust thin film systems up to 600°C
- Porosification/Etching techniques
- LTCC/ceramics, flex, silicon, sapphire

- **Device related activities:**
- Viscosity/density MEMS sensor
- Energy harvesting devices
- High temperature (pressure) sensors
- RF-MEMS switch
- Flow sensors

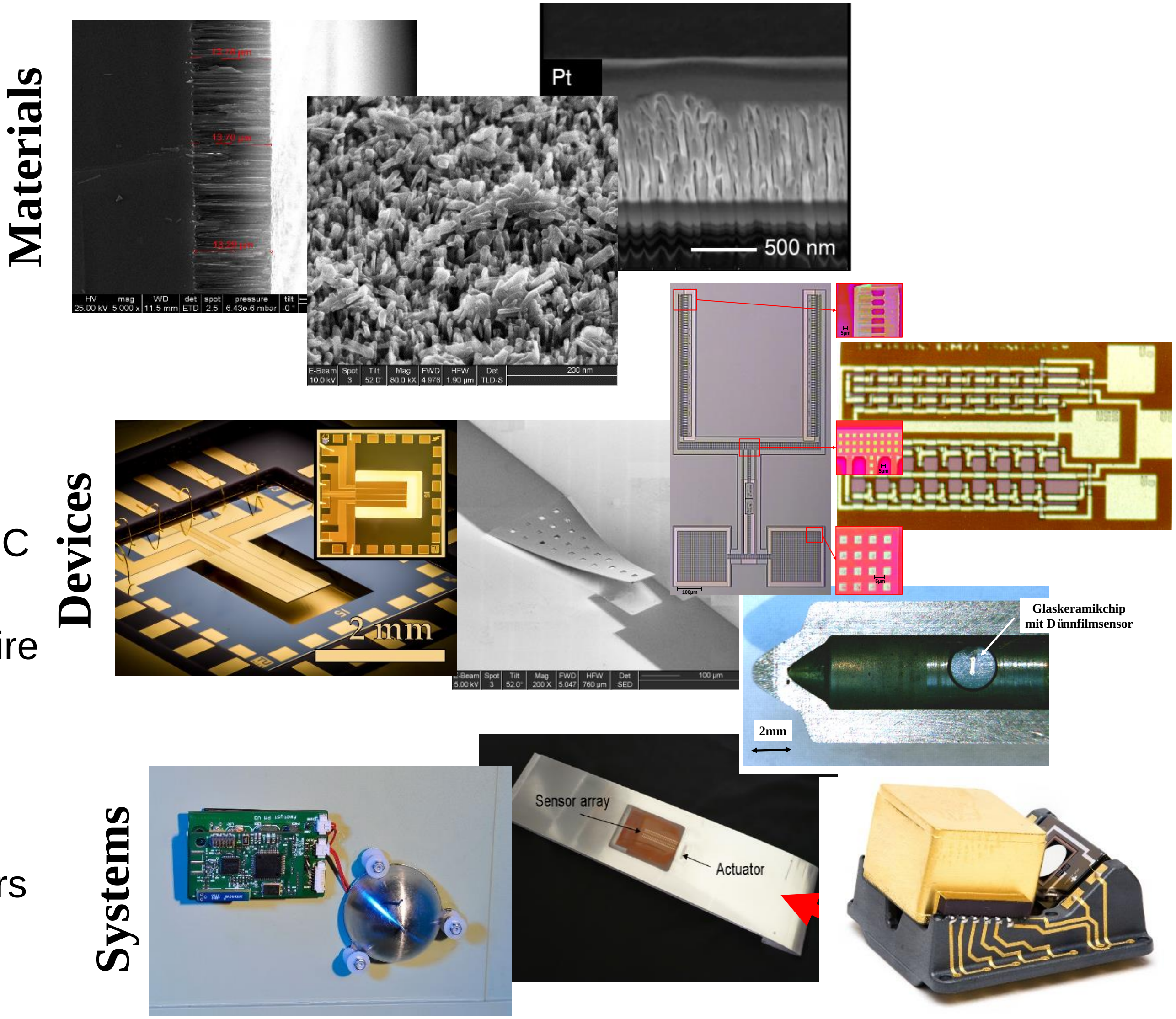

Research topic:

AlN/ScAlN Thin Film Properties

Motivation: Piezoelectric thin films in MEMS

Typical application scenarios in electronic devices, sensors and actuators:

- **SAW:** Two port delay line and resonator (b) based sensors [1]
- **RF – Switches** based on PZT actuators (a) [2]
- **Cantilever** based accelerometers (c) [2], gyroscopes [3]
- **Cantilever** based detection of adsorbed masses, viscosity, molecules (d) [4]

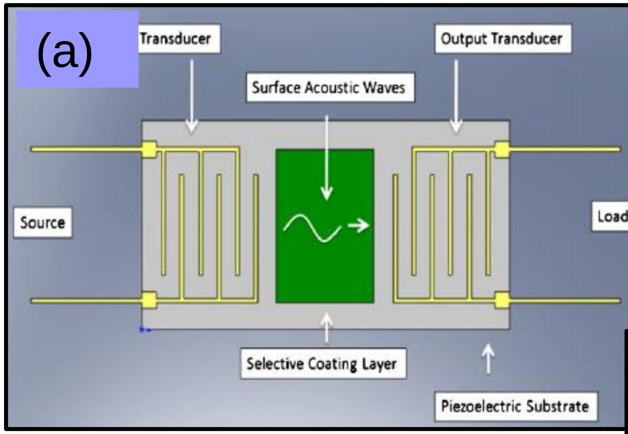

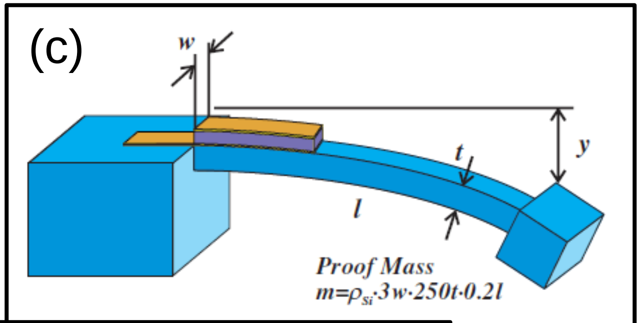

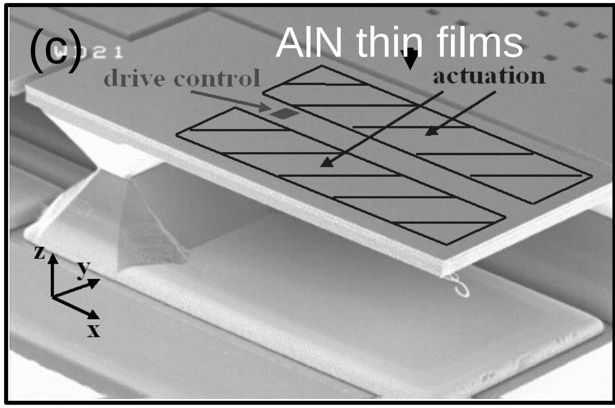

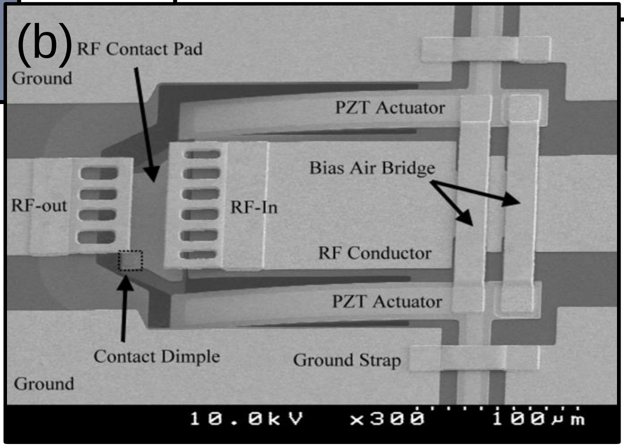

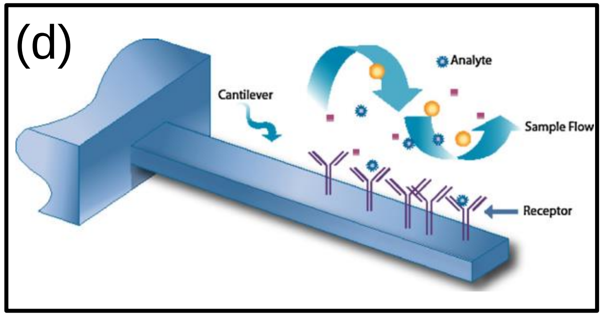

[1] Tadigadapa, S. and K. Mateti (2009). "Piezoelectric MEMS sensors: state-of-the-art and perspectives." Measurement Science & Technology **20(9)**; [2] Polcawich R (2007) *PhD Thesis,* Pennsylvania State University; [3] S. Günthner, M. Egretzberger, A. Kugi, K. Kapser, B. Hartmann, U. Schmid und H. Seidel; IEEE Sensors Journal, Vol. 6, No. 3, pp. 596 – 604, 2006. [4] Tamayo, J., et al. (2013). "Biosensors based on nanomechanical systems." Chemical Society Reviews **42(3): 1287-1311.**

Piezoelectric Effect

- Change of electrical polarization due to mechanical deformation of solids

  → **direct piezoelectric effect**
- Deformation due to applied electric field

  → **converse piezoelectric effect**

- **Non-centrosymmetric** crystal structure (not having a centre of symmetry)

- **Common materials:**
  - Crystals (quartz, LiNiO3, GaPO4,…)
  - Ceramic thin films (PZT, AlN, ZnO,…)
  - Polymers (PVDF,…)

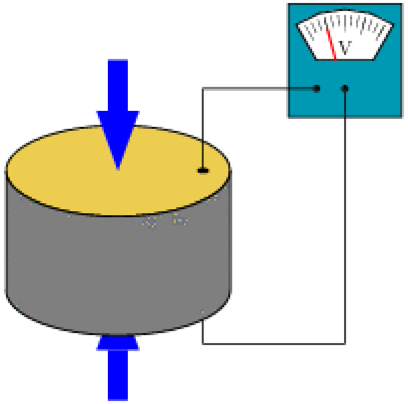

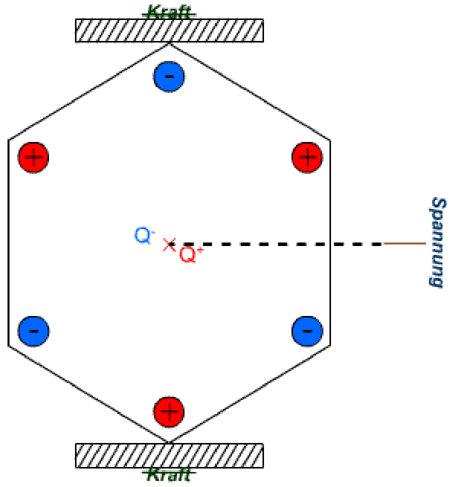

https://en.wikipedia.org/wiki/Piezoelectricity
https://de.wikipedia.org/wiki/Piezoelektrizit%C3%A4t

Mathematical description of piezoelectric effect:

Mechanical stress

$$T_i = c^E_{ij} S_j - \boxed{e_{mi} E_m}$$

Mechanical strain

$$S_i = \underbrace{s^E_{ij} T_j}_{\text{pure mechanical}} + \underbrace{\boxed{d_{mi} E_m}}_{\text{electro mechanical coupling}}$$

Motivation: Comparison of Piezoelectric Thin Film Materials

- **Most typically used piezoelectric thin films in MEMS devices:**
  - PZT (Pb (Zr, Ti) O_3) → ferroelectrica, various compositions
  - BCZT → ferroelectrica, various compositions
  - ZnO, AlN → piezoelectrica

- **Important electromechanical properties:**

Material	ε_r	d_{31} / pm/V	d_{33} / pm/V	C / ms^{-1}
AlN	10.0	-2.5	5	6000
PZT(25/75, 50/50)	300/165	-15/-12	33/27	2700
BCZT	1000.0	-40.0	80	
ZnO	10.9	-5.8	11	6000

Motivation: AlN related Properties

Material Properties

- ❖ AlN is piezoelectric
- ❖ Direct wide band gap **(6.2 eV)**
- ❖ Good electrical isolation **(4-12 MV/cm breakdown field)**
- ❖ Low dielectric constant ε_r (~10 ε_0)
- ❖ Relative high thermal conductivity **(20...300 W/mK)**
- ❖ High temperature stability
- ❖ High acoustic wave velocity (~ 6000 m/s)
- ❖ Good temperature stability

Device Related Properties

- ❖ Low piezoelectric coefficients ☹
- ❖ CMOS compatible, lead free ☺
- ❖ Requires no high temperature poling step ☺

Crystal structure

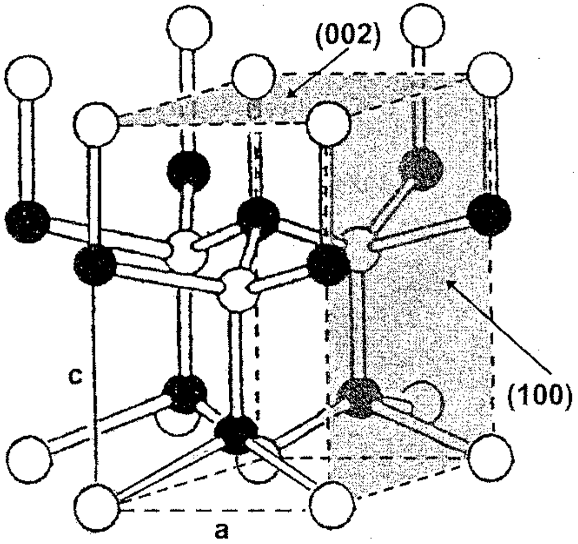

Hexagonal wurtzite
a: 3.110 Å
c: 4.980 Å

(002) basal plane is the most closed packed plane

Introduction: Film Synthetization I

Various deposition techniques reported in literature such as

- ADL
- Pulsed laser deposition
- MOCVD
- MBE
- **Sputter deposition (DC, RF)**

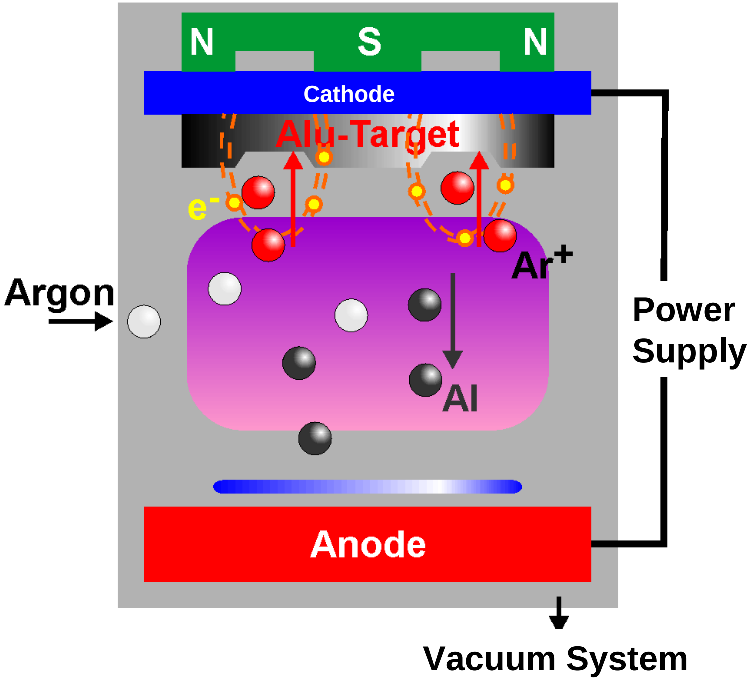

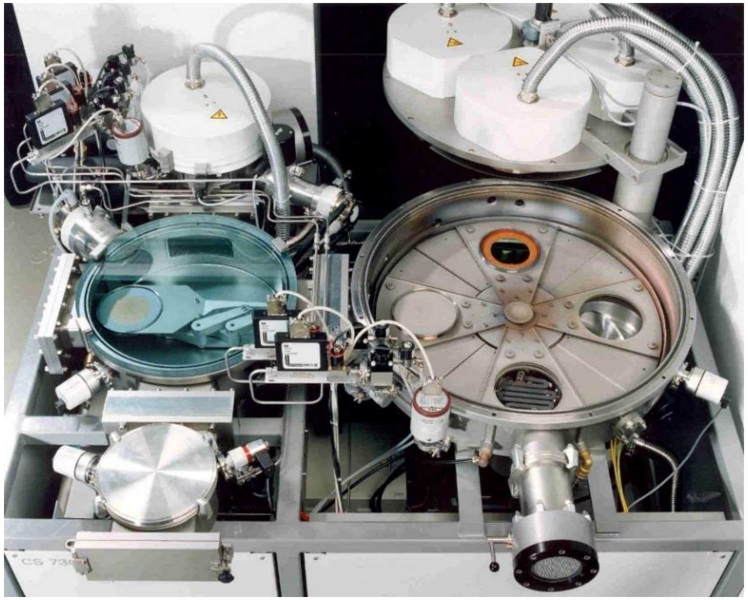

- DC reactive magnetron sputtering system
- Silicon substrates (100), substrates nominally unheated
- Film deposited at different back pressures, plasma powers and gas compositions (N_2/Ar ratio), electrode distance
- Purity of aluminium target: 99.999%
- Diameter of aluminium target: 150 mm
- Distance between target and substrate: range several cm

Introduction: Film Synthetization II

Typical AlN layer from our deposition equipment

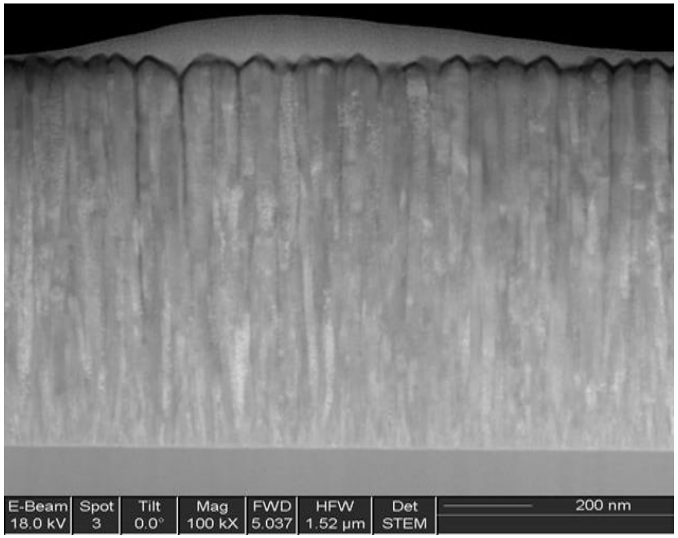

1000W, 4e-3mbar, 100%N2

Typical example from other groups:

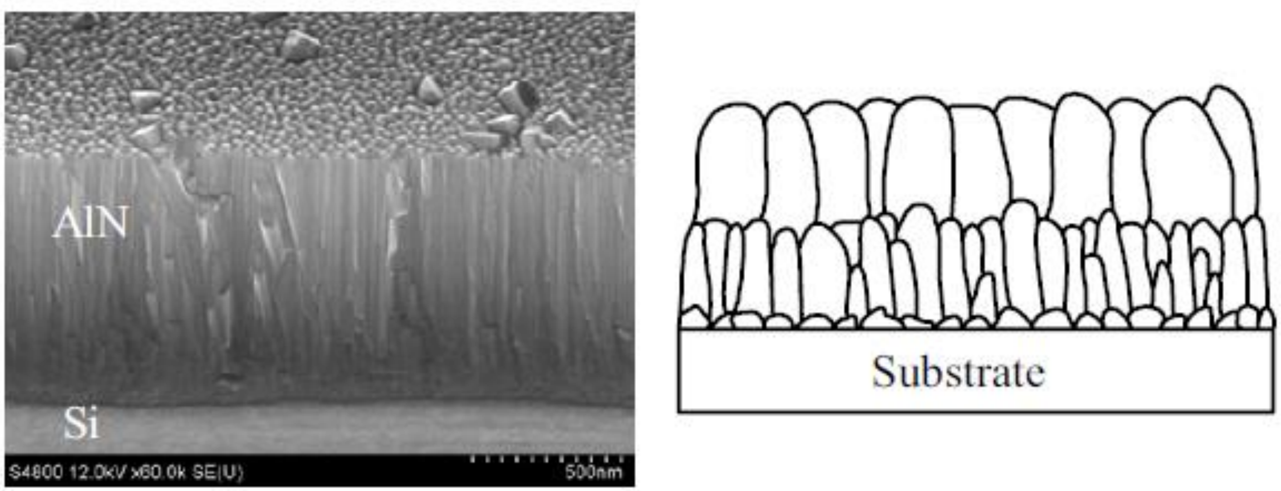

Figure 1. Left: scanning electron microscope (SEM) picture of the texture gradient of an AlN film; right: schematic cross section of a thin nanocrystalline aluminum nitride film.

Mehner et al., JMM, 23 (2013) 095030 (9pp).

Sputter-deposited AlN layers are polycrystalline!

Wet Chemical Etching Experiments I

SEM analysis – Low c-axis orientation

Film deposited at 500 W, $6 \cdot 10^{-3}$ mbar and 75% N_2 (25% Ar)

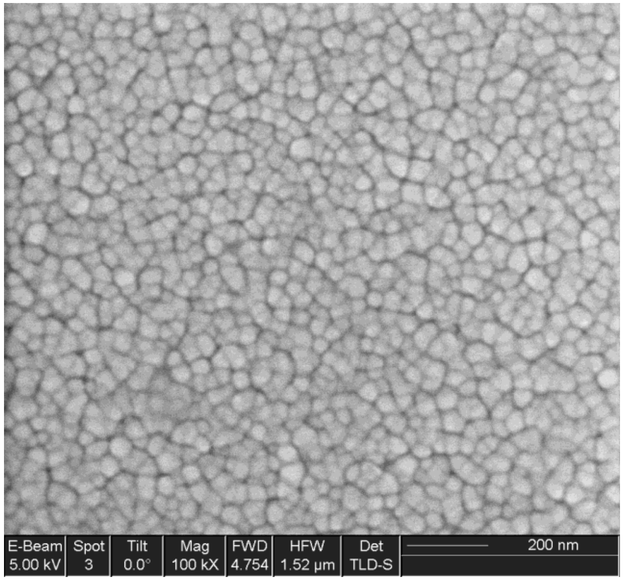

Surface morphology
“as-deposited”
Grain size: ~30 nm

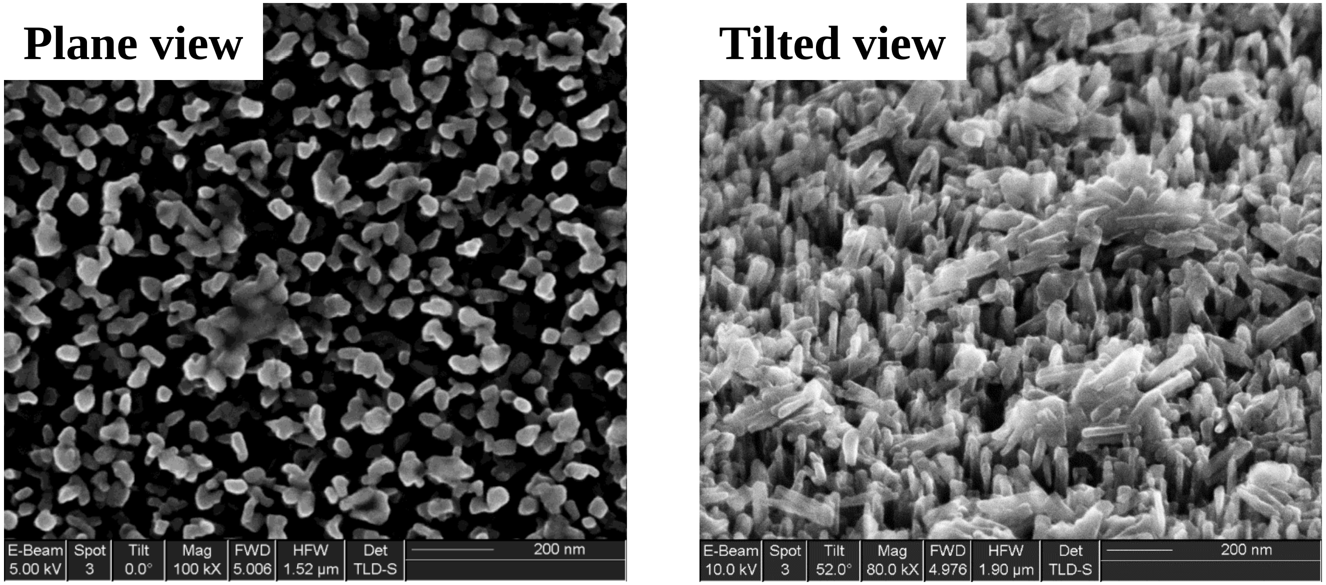

Surface morphology
after 5 s in H_3PO_4 at 80°C
Etch rate: 743,7 Å/s

Surface porosity is very high

Wet Chemical Etching Experiments II

SEM analysis – High c-axis orientation

Film deposited at 1000 W, $4 \cdot 10^{-3}$ mbar and 100% N_2 (0% Ar)

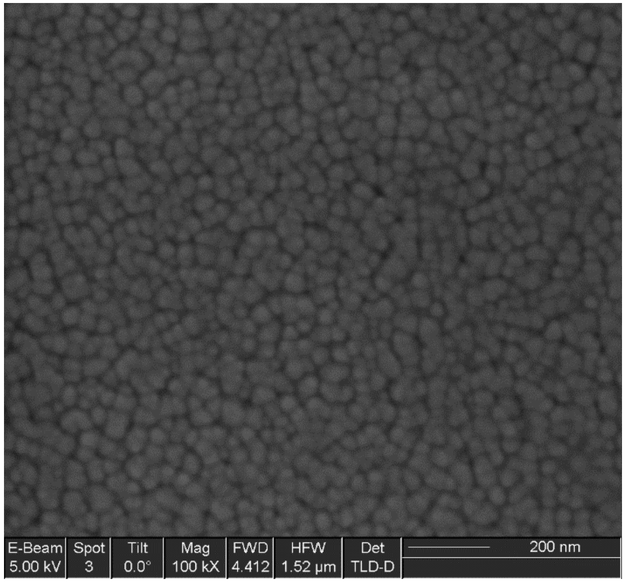

Surface morphology
“as-deposited”
Grain size: ~ 30 nm

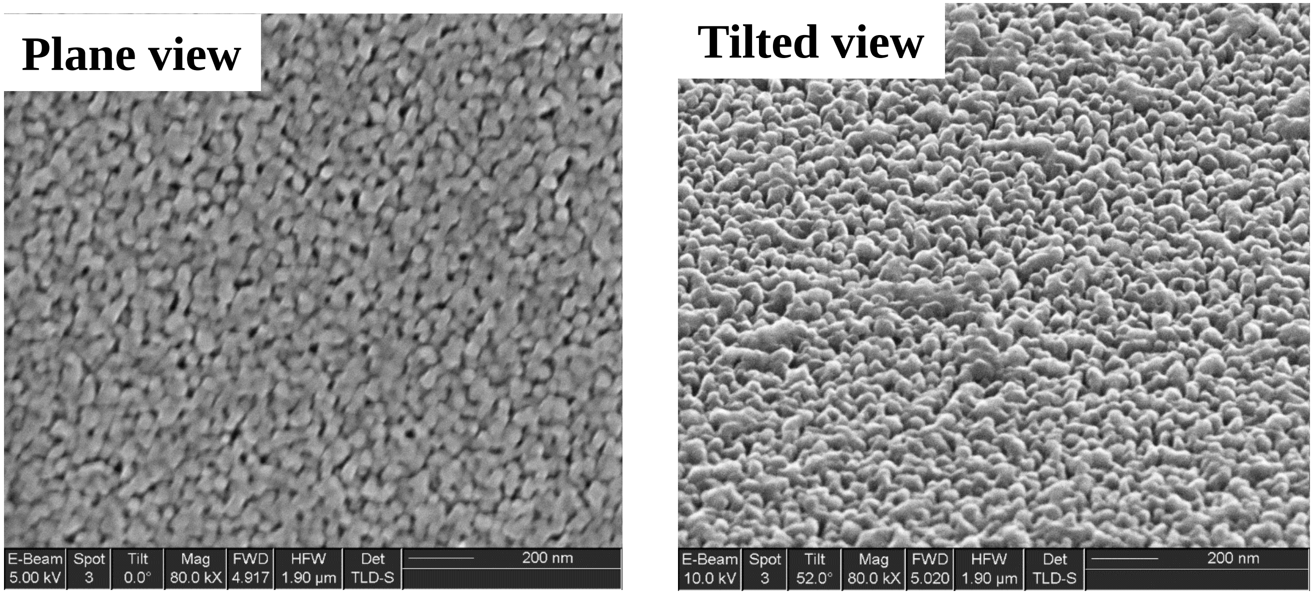

Surface morphology
after 20 s in H_3PO_4 at 80°C
Etch rate: 135 Å/s

Mean grain size is unaffected

Surface porosity is low

XRD Analyses

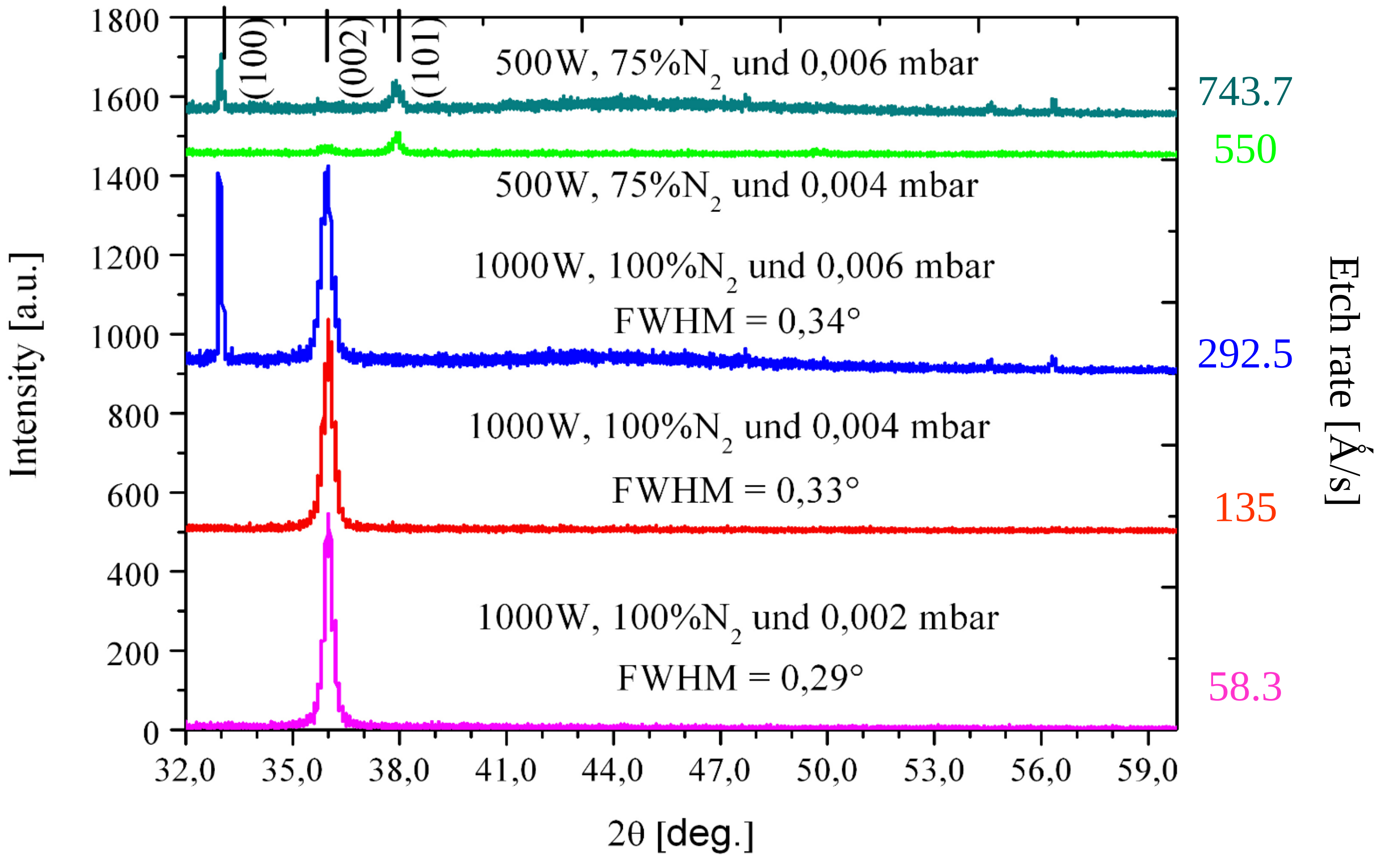

C-axis orientation↑(Intensity↑, FWHM↓) → Etch rate↓

(002) basal plane is the most closed packed plane

A. Ababneh, H. Kreher und U. Schmid; *Etching Behaviour of Sputter-Deposited Aluminium Nitride Thin Films in H_3PO_4 and KOH Solutions;* **Microsystem Technologies, Vol. 14, No. 4-5, pp. 567-573, 2008.**

Determination of Piezoelectric Coefficients

FEM-simulations (d_{33}= 5.5pm/V; d_{15}= 4pm/V)

Test structure

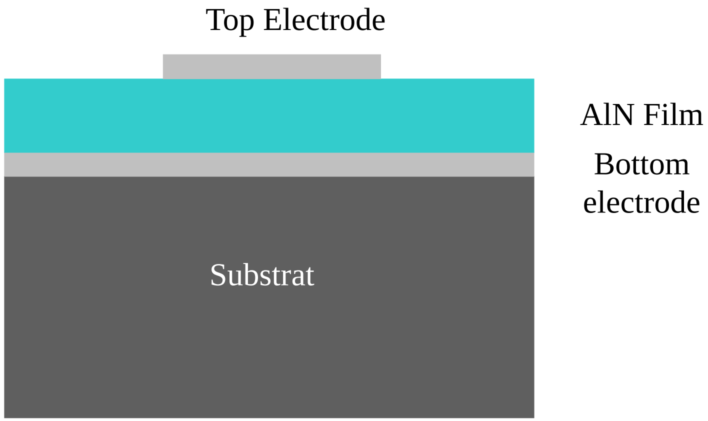

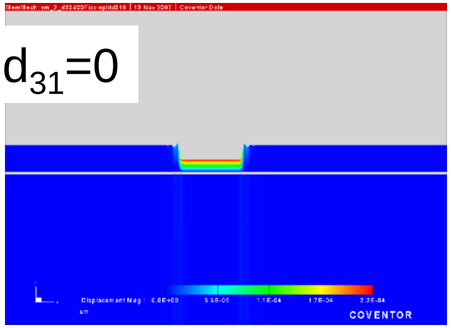

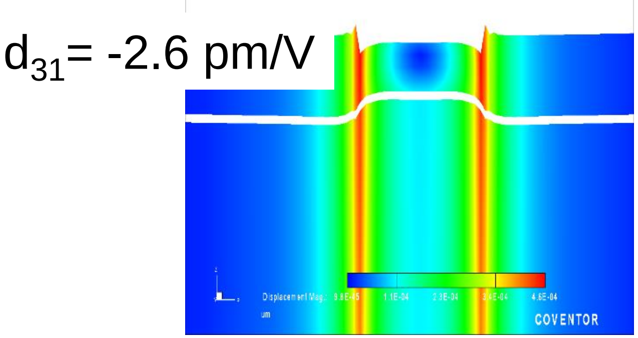

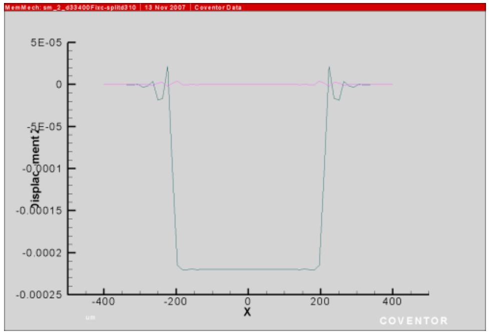

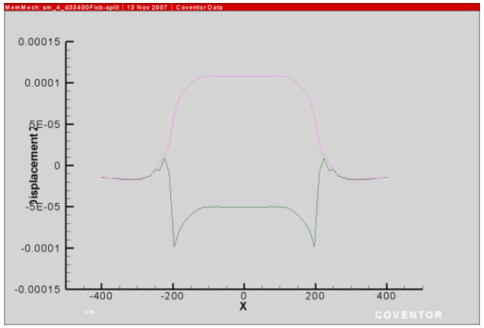

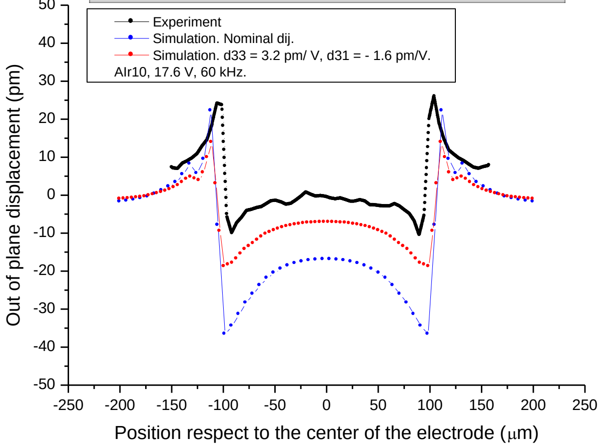

Assumption:

d_{31}= -d_{33}/2

J. Hernando, J.L. Sánchez-Rojas, E. Iborra, A. Ababneh and U. Schmid,
Simulation and laser vibrometry based characterization of piezoelectric AlN thin films;
Journal of Applied Physics, Vol. 104 pp. 053502, 2008.

Mechanical Characterization using Bulge Testing I

- Uniform pressure load
- Displacement is measured
- Describe bending behavior by polynomial

$$w(r,\boldsymbol{\alpha}) = w_0 \sum_{k=0}^{K} \alpha_{2k} \left(1 - \left(\frac{r}{R}\right)^2\right) \left(\frac{r}{R}\right)^{2k}$$

→ Coefficients determined by bending behaviour

→ Applying minimum potential energy approach for C_i determination

$$p(w_0) = C_1(\boldsymbol{\alpha}) \frac{\sigma_f d w_0}{R^2} + C_2(\boldsymbol{\alpha}; \upsilon) \frac{Y d w_0^3}{R^4}$$

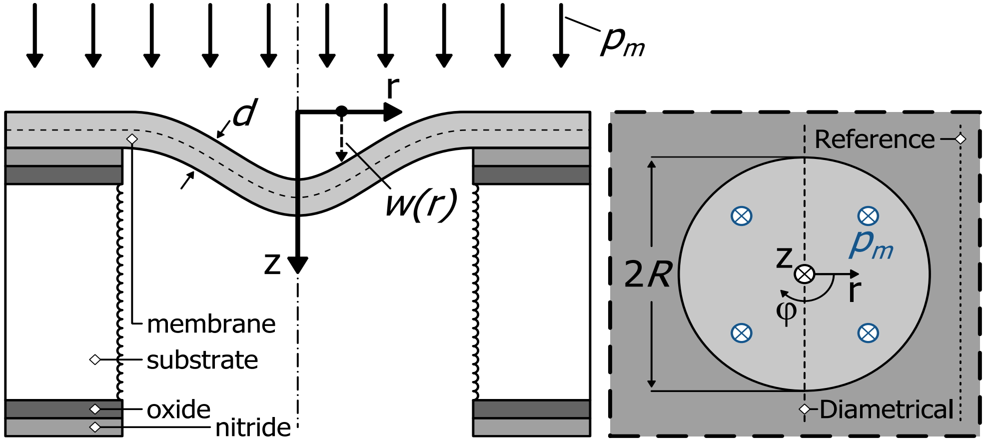

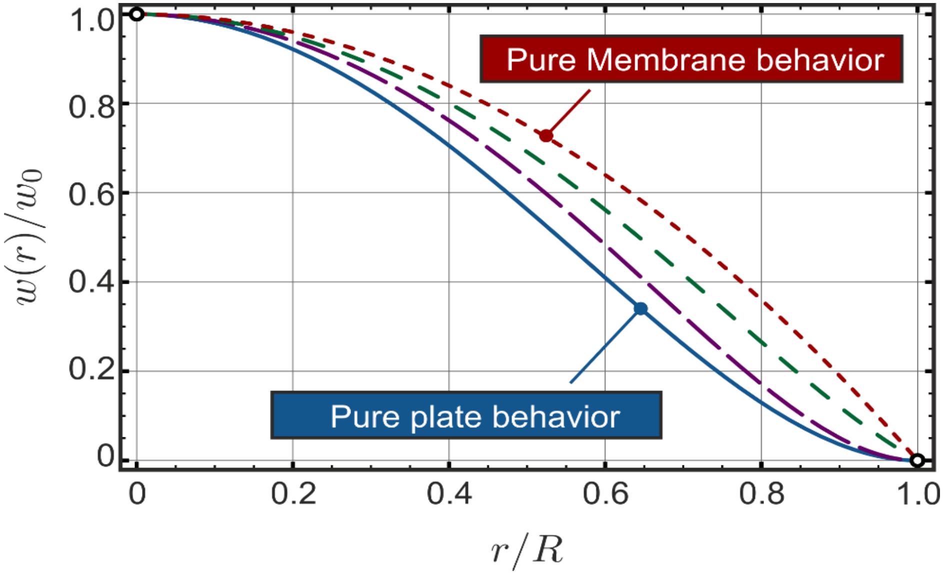

R. Beigelbeck et al., Journal of Applied Physics, Vol. 116, pp. 114905, 2014.

Mechanical Characterization using Bulge Testing II

Experimental verification of novel mathematical model using a **silicon** membrane

→despite non-standard bending curve shape

→excellent agreement with predicted value (E=179,5GPa, σ=110MPa)

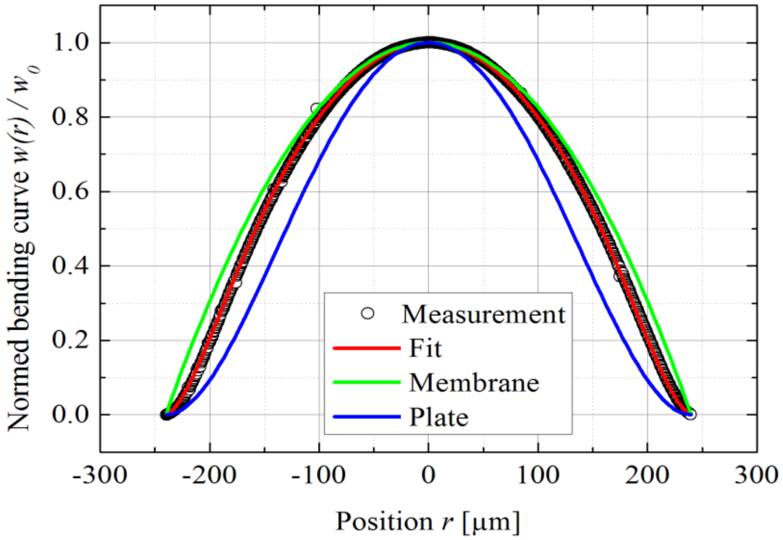

Analysis of AlN membranes with thicknesses ranging from 1.2 µm down to about 120 nm

- Low variation with film thickness
- Close to results from nano indentation

Isoptropic Young`s Modulus

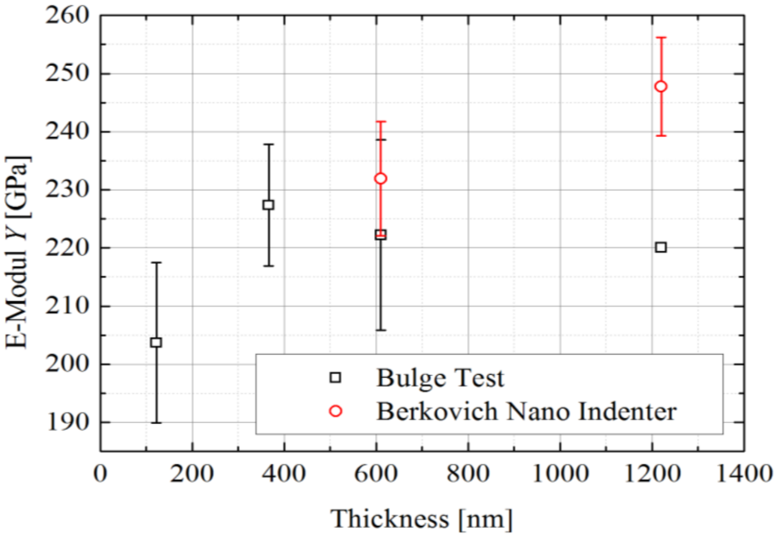

M. Schneider *et al.*, Applied Physics Letters, Vol. 105, pp. 201912, 2014.

Silicon Surface Pre-Conditioning Using Sputter Etching I

Original

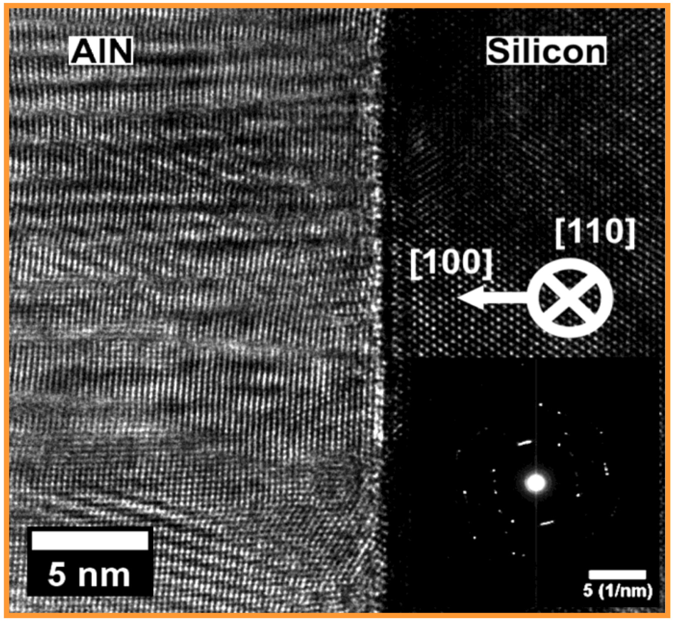

Modified

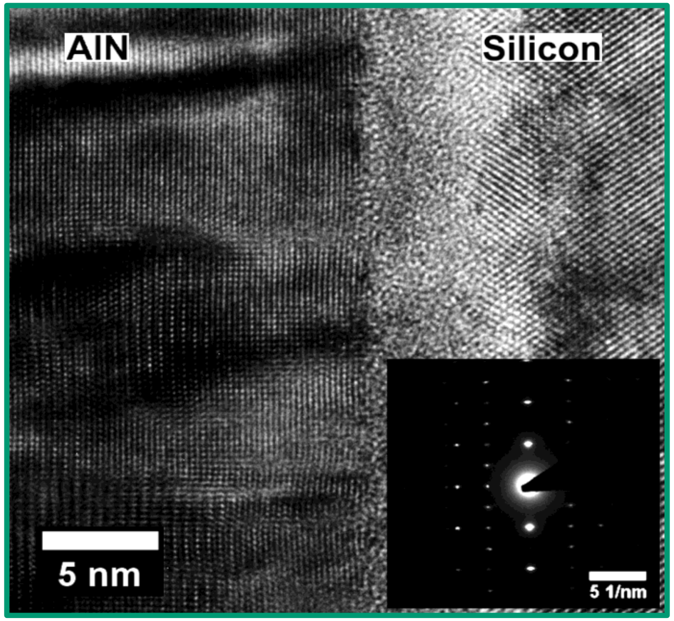

- Forming of a ~6 nm thick layer of **amorphous silicon**
- Consistent with simulations of Ar-ion penetration depth
- Introduction of **surface-near nucleation sites**
- Significant increase in film quality at the **same deposition parameters**

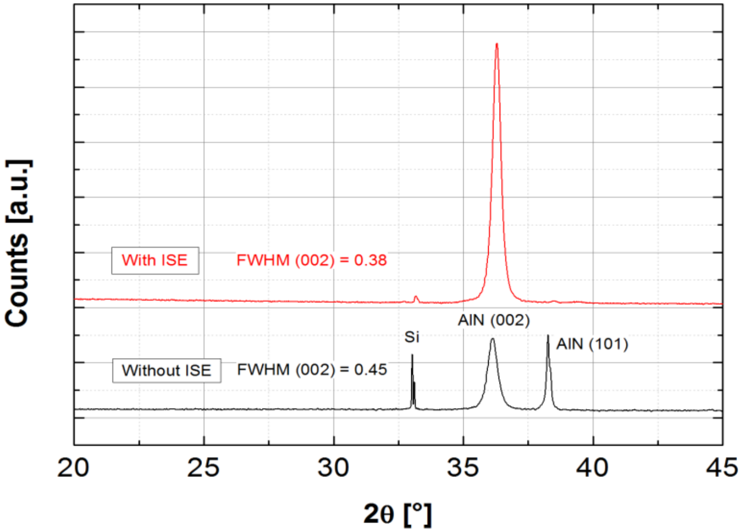

M. Schneider, et al., Applied Physics Letters, Vol. 101, p. 221602, 2012.

Silicon Surface Pre-Conditioning Using Sputter Etching II

- Prior to sputter deposition, the silicon substrate is sputter etched for 5min

- Significantly lower leakage currents are observed for the **pre-treated sample** in comparison to a **reference sample**

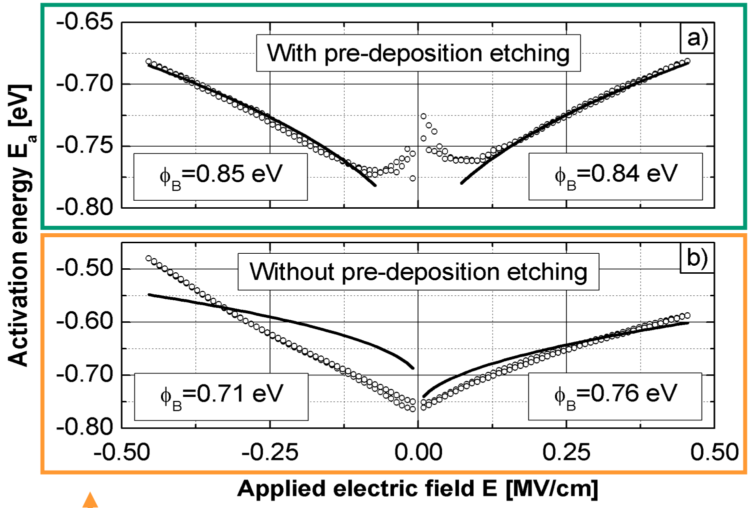

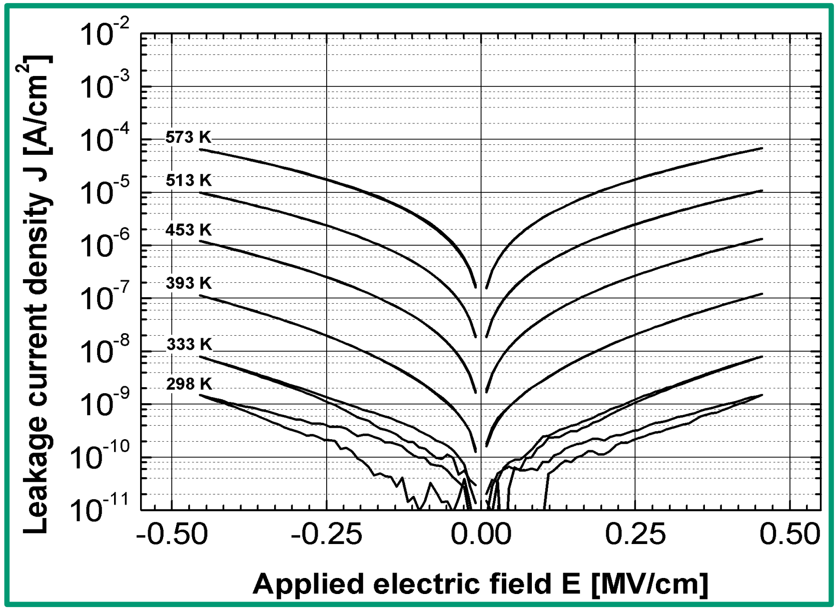

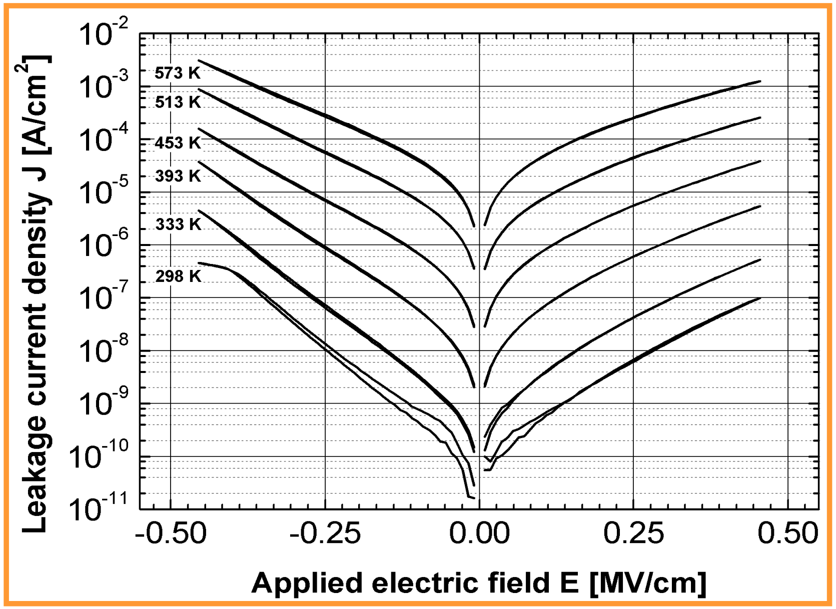

Tailoring the silicon / AlN interface II

- **As expected: linear correlation between d_{33} and d_{31}**

$$\rightarrow d_{31} = -0.389 d_{33}$$

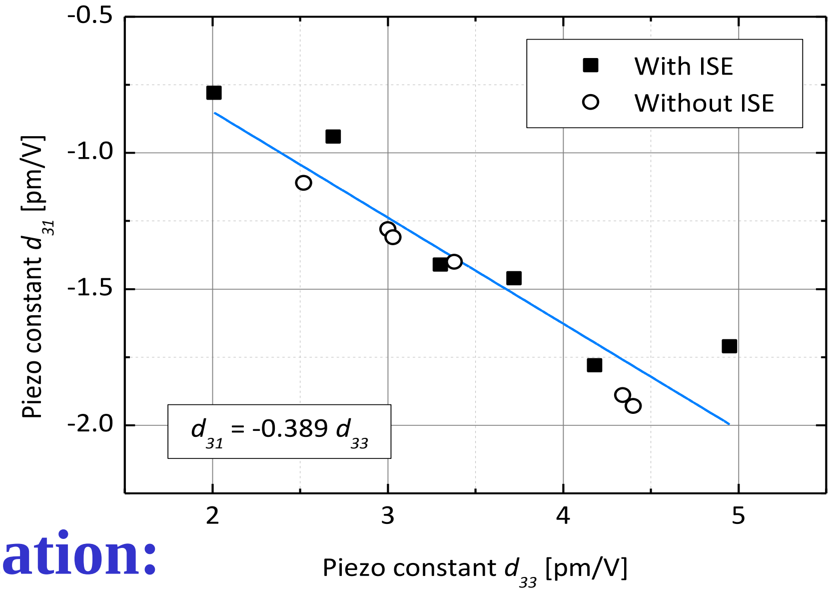

Alternative technique for d_{33} determination:


Piezometer PM300

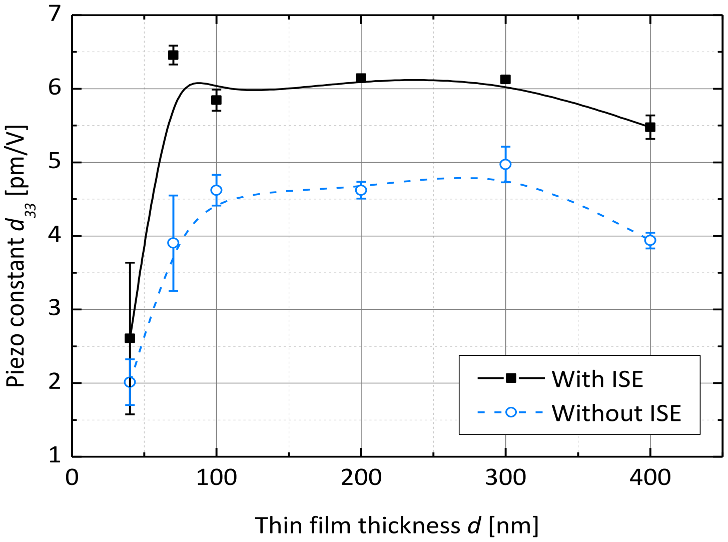

M. Schneider et al., Journal of Physics D: Applied Physics, Vol. 48, pp. 405301 (7pp), 2015.

Transition Metal Doping of AlN

Improvement of piezoelectric constant d_{33}:

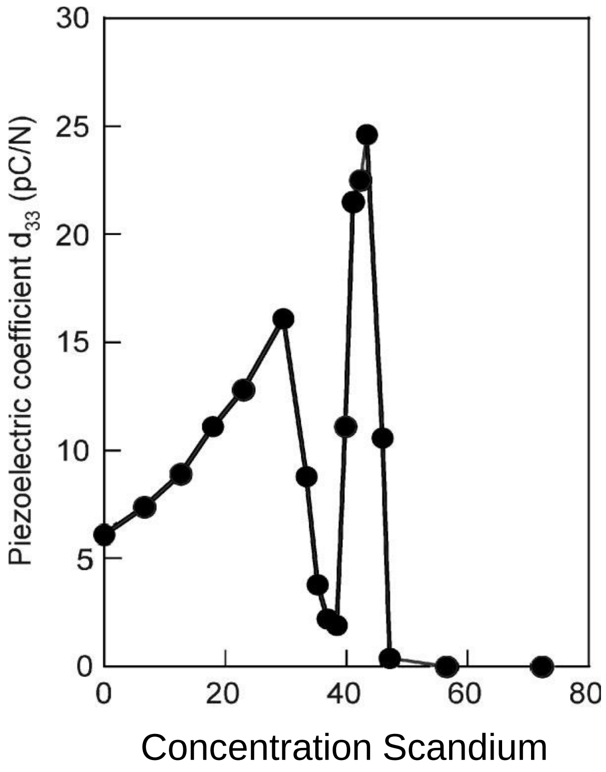

- 2 port excitation, 180° phase shifted: 10V, 10-100kHz
- LDV Measurement compared to 3 FEM simulations
- Accuracy of extraction of d_{33} and d_{31} improved

  → Via plateau shape comparison

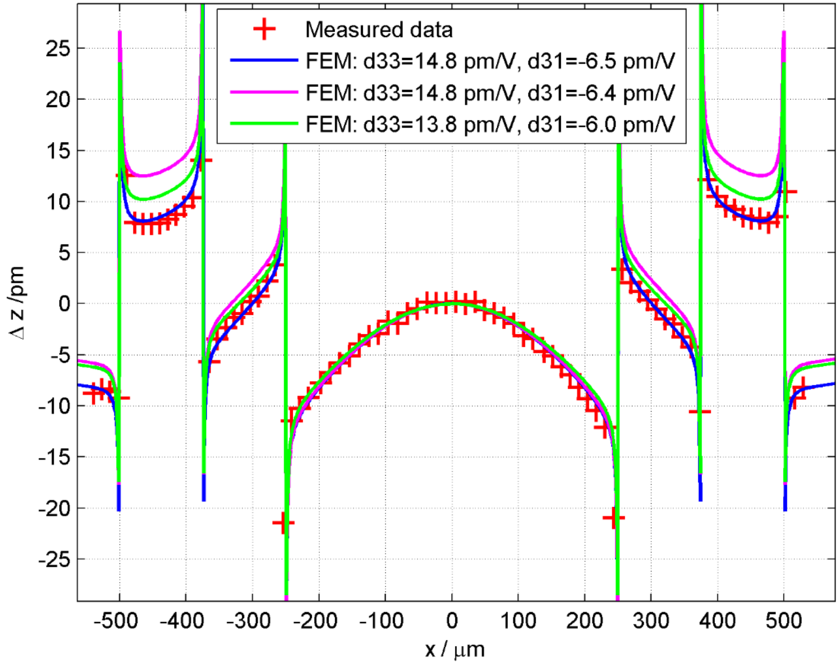

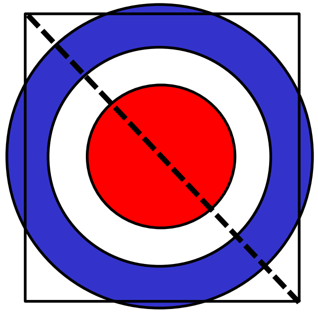

High Accuracy in d_{31} and d_{33} determination

M. Akiyama et al., Adv. Mater. 2009

P. Mayrhofer et al., Sensors&Actuators A, Vol. 222, pp. 301-308, 2015.

Piezoelectric constants of $Y_xAl_{1-x}N$

Piezoelectric constant d_{33}:

- slight increase up to x = 6% Yttrium
- below theoretical value

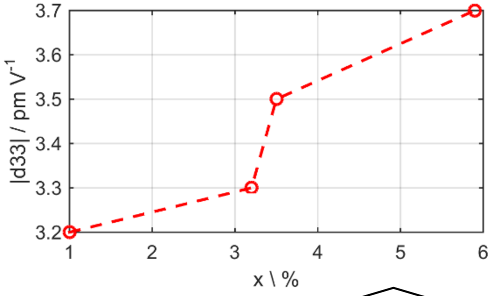

Measured d_{33} at highest c-axis orientation of $Y_xAl_{1-x}N$

Amorphous initial growth layer found in TEM analysis

→ Thickness increases with Yttrium

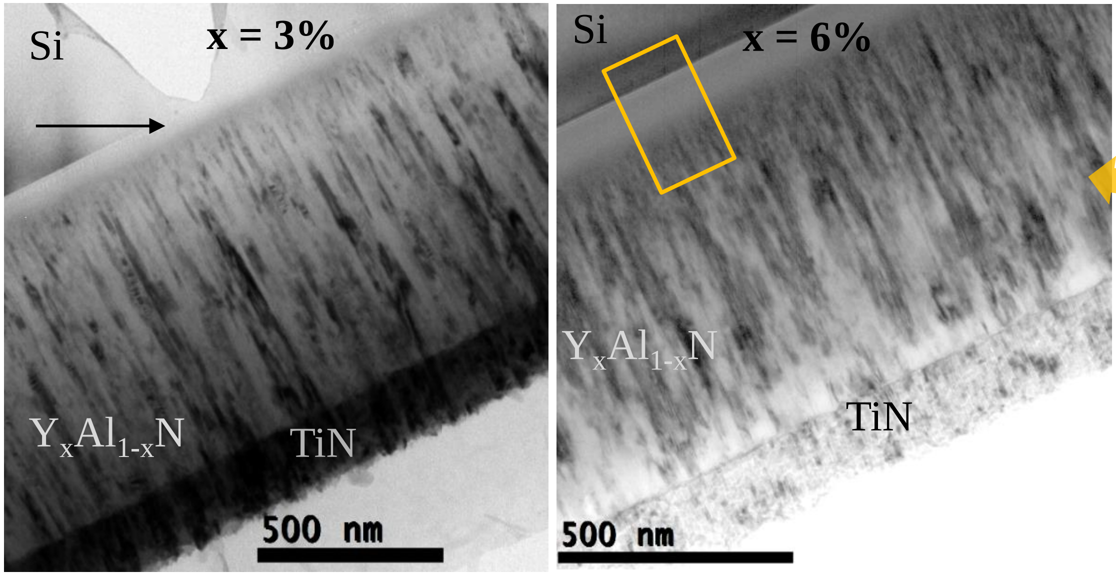

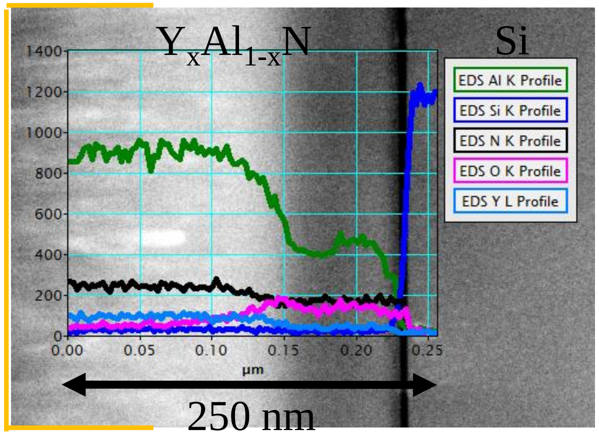

EDX elemental profile scan for x = 5.8%

Mayrhofer, P. M., et al., Acta Materialia, Vol. 100, pp. 81-89, 2015.

Research topic:

Piezoelectric Resonators

MEMS Resonators: Cantilever Manufacturing Process

a) SOI (silicon on insulator) wafer with 20 µm device silicon thickness and coating of SiO_2 and SI_3N_4

b) Deposition of Cr/Au electrode, piezoelectric AlN layer and Al top-electrode

- patterning of AlN with a lift-off process using titanium as sacrificial layer and 40% hydrofluoric acid (HF)

c) Patterning of cantilever and backside hole by DRIE etching process

d) Cantilever release by BOX (burried oxide) removing with 5% buffered HF acid

dicing, mounting, bonding,…..

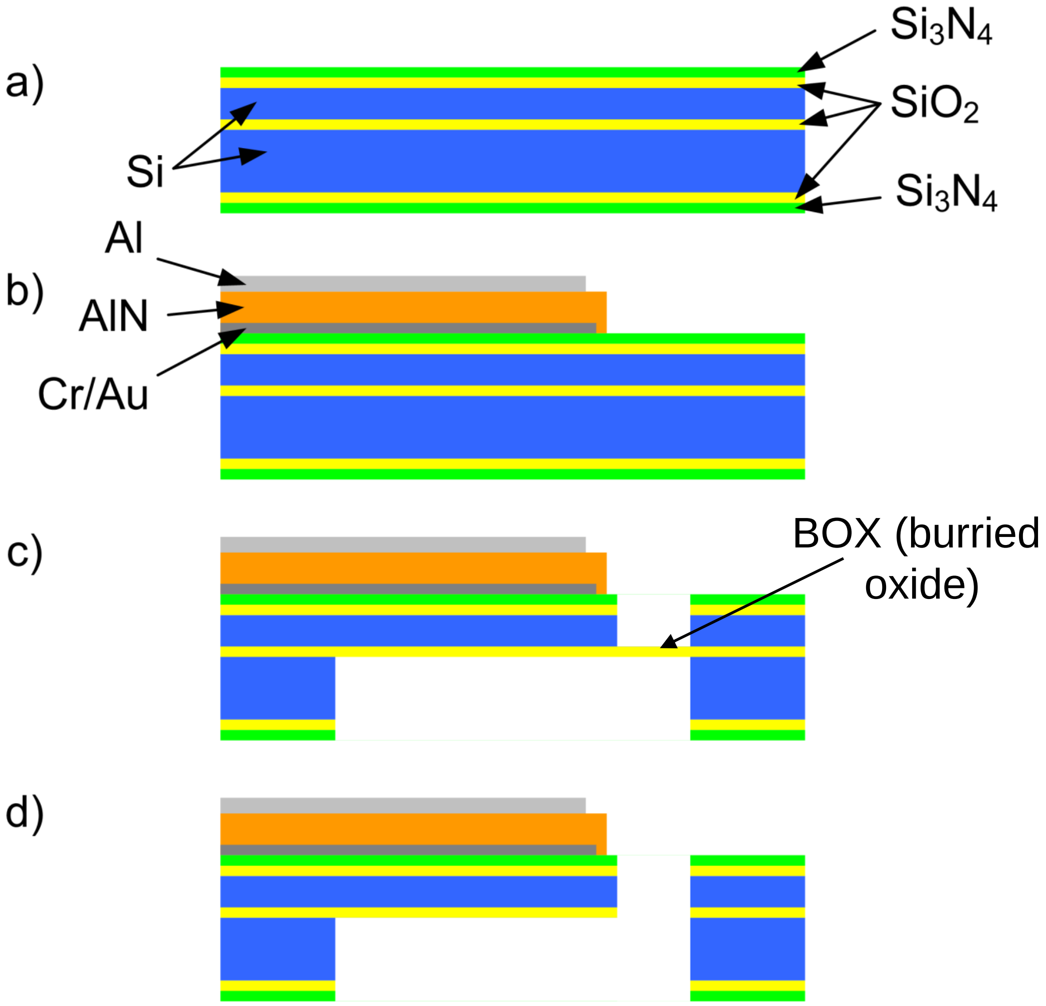

M. Kucera et al., *Q-factor enhancement of a self-actuated self-sensing piezoelectric MEMS resonator applying a lock-in driven feedback loop*, **J. Micromech. Microeng. 23 (2013) 085009.**

Basic Device & Fluid Properties

Modified Butterworth-Van Dyke equivalent circuit

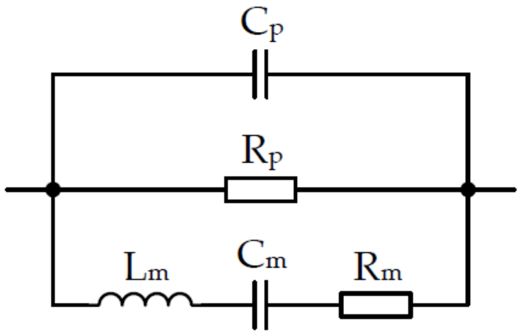

C_p … Parallel capacitance

R_p … Leakage resistance

R_m, L_m, C_m … Mechanical resonance

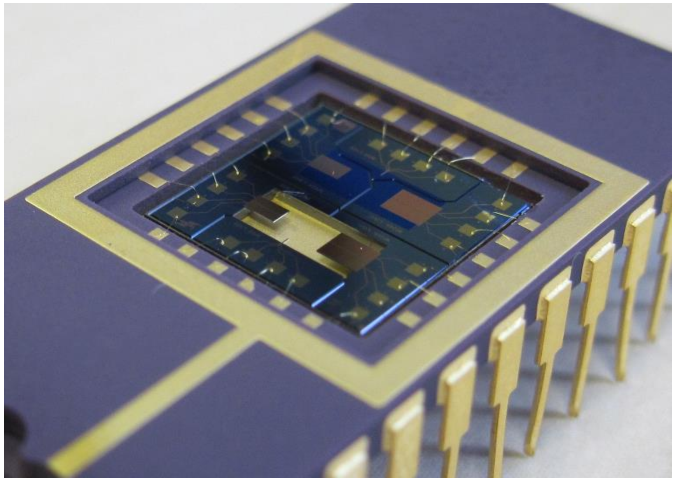

Comparison between Cantilever and Dummy Structure - G and B

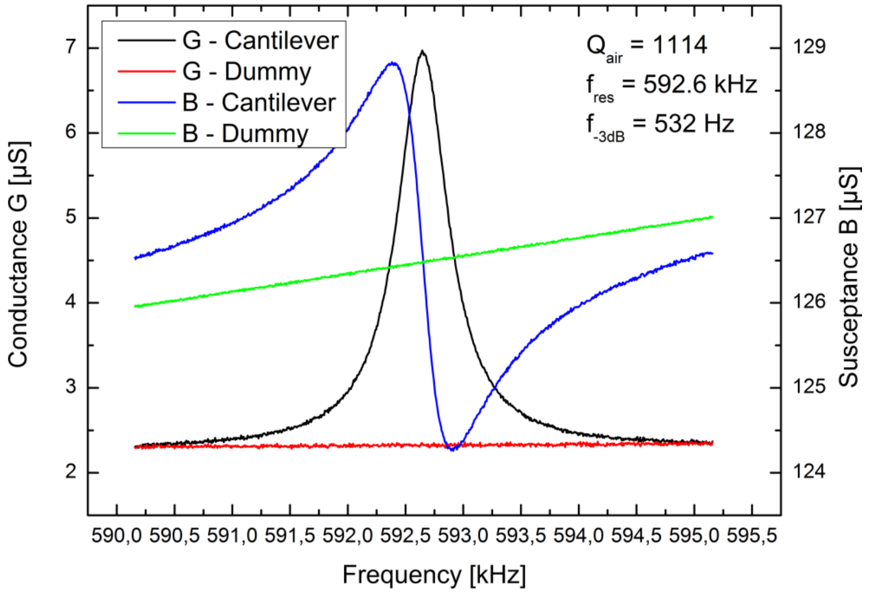

Fluid properties

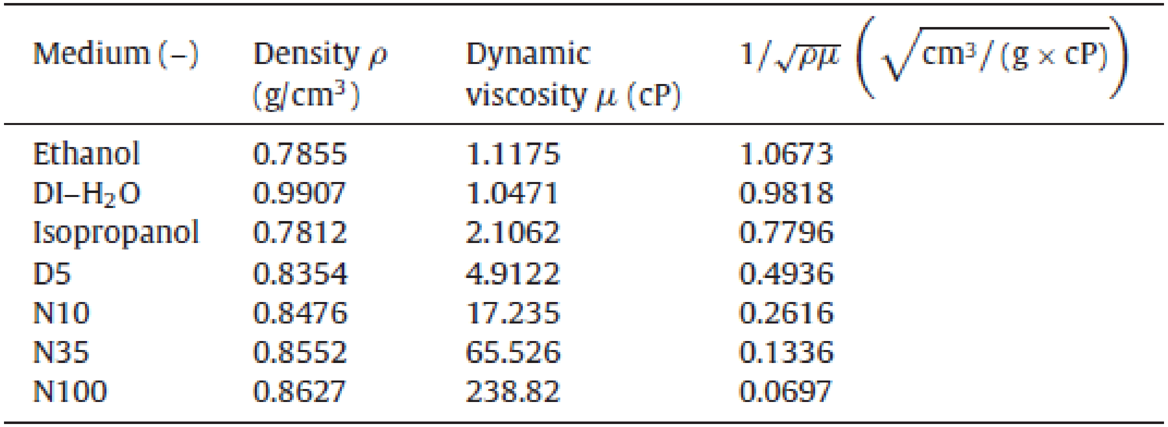

Medium (–)	Density ρ (g/cm^3)	Dynamic viscosity μ (cP)	$1/\sqrt{\rho\mu}$ $\left(\sqrt{\text{cm}^3/(\text{g} \times \text{cP})}\right)$
Ethanol	0.7855	1.1175	1.0673
DI–H_2O	0.9907	1.0471	0.9818
Isopropanol	0.7812	2.1062	0.7796
D5	0.8354	4.9122	0.4936
N10	0.8476	17.235	0.2616
N35	0.8552	65.526	0.1336
N100	0.8627	238.82	0.0697

Viscous Damping in Liquids

- **Viscosity is defined as:**
  - μ_f …dynamic viscosity
  - τ …shear stress
  - S …shear rate

$$\mu_f = \frac{\tau}{S}$$

$$S = \frac{\partial v}{\partial z} = \frac{v_x}{d}$$

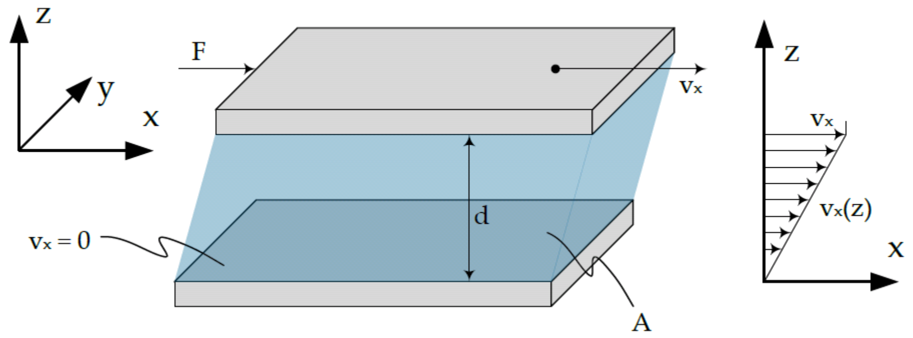

- **Cantilever in liquid is approximated by sphere**
  - Kinetic energy and dissipated energy can be analytically calculated for a sphere in liquids
  - Q-factor is defined as $Q = 2\pi\, E_{kin}/E_{diss}$

→ $$\boxed{Q = \frac{\rho_c WTL\sqrt{\omega}}{3\pi R_{eq}^2 \sqrt{2\mu_f \rho_f}}}$$

- ρ_c … density of cantilever
- W, T, L … width, thickness, length of cantilever
- ω … resonance frequency
- R_{eq}^2 … equivalent sphere radius (approx. cantilever surface *WL*)
- $\sqrt{\mu_f \rho_f}$ … sqrt of density viscosity product

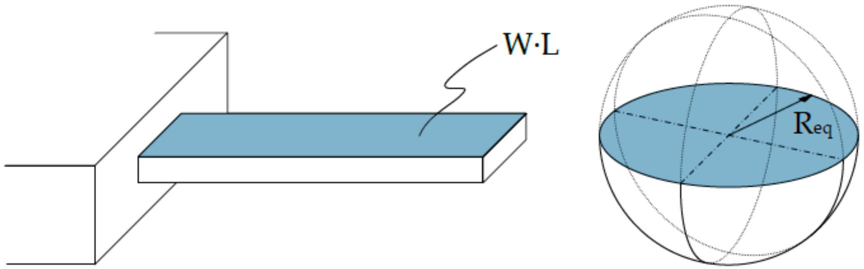

Study on the In-Plane Vibration Mode I

- In-plane bending mode
- Vacuum ⇒ Q ~ 5527 (electr.)
- Air ⇒ Q ~ 3274 (electr.)
- Isoprop. ⇒ Q ~ 13 (optical)

⇓

  - Estimated peak ΔG ~ 18 nS
  - B ~ 63.9 µS imaginary part

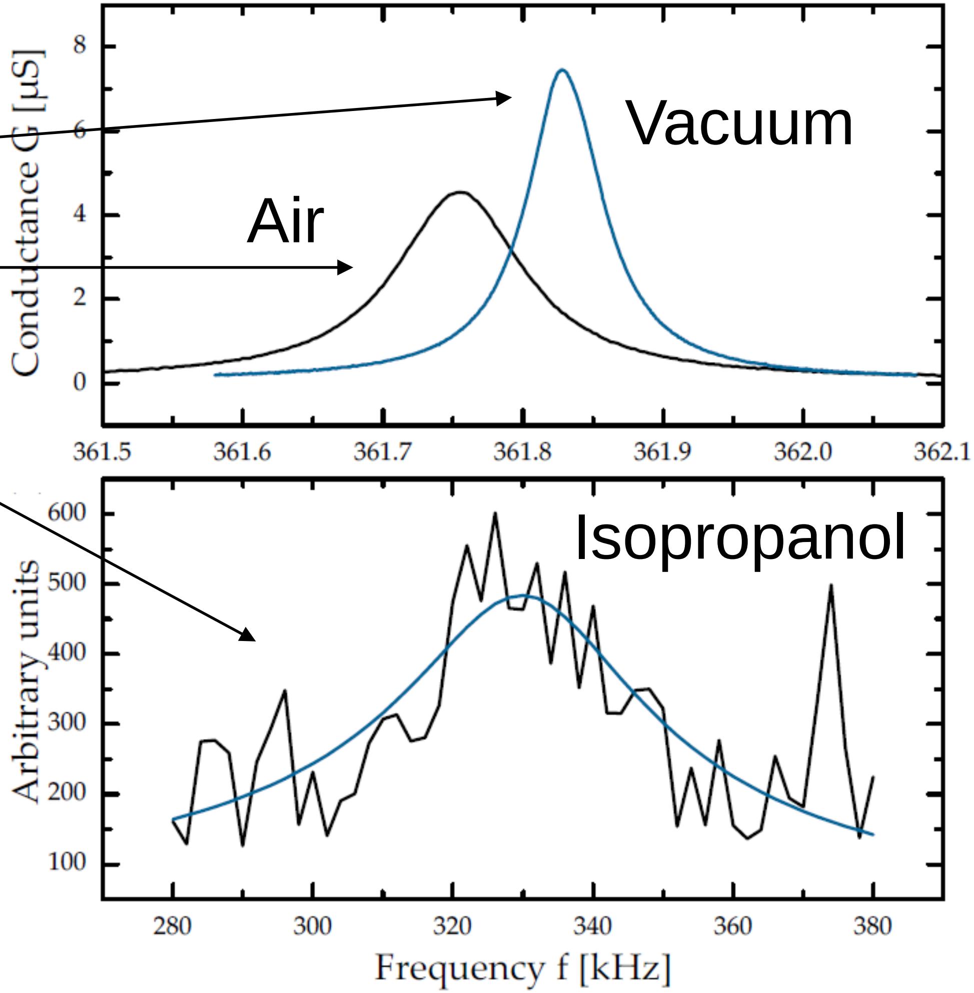

Resonance electrically not detectable!

⇒ **Piezoelectric area is too small!**

Study on the In-Plane Vibration Mode II

Need to evaluate the piezoelectric area @ equal resonance frequency!

- Different sized cantilevers with $\omega_1 = \lambda_1^2 \frac{W}{L^2}\sqrt{\frac{E_c}{12\rho_c}}$
- AlN area scaling factor α

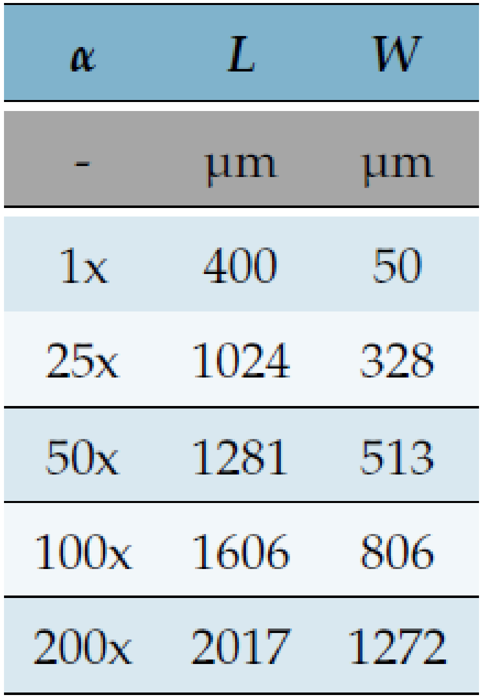

α	L	W
-	µm	µm
1x	400	50
25x	1024	328
50x	1281	513
100x	1606	806
200x	2017	1272

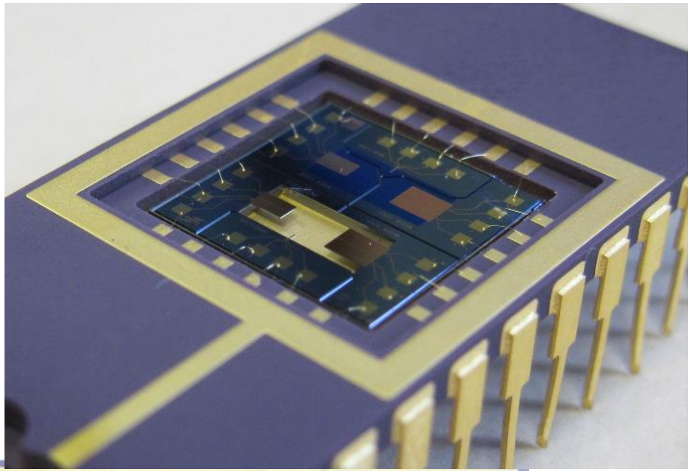

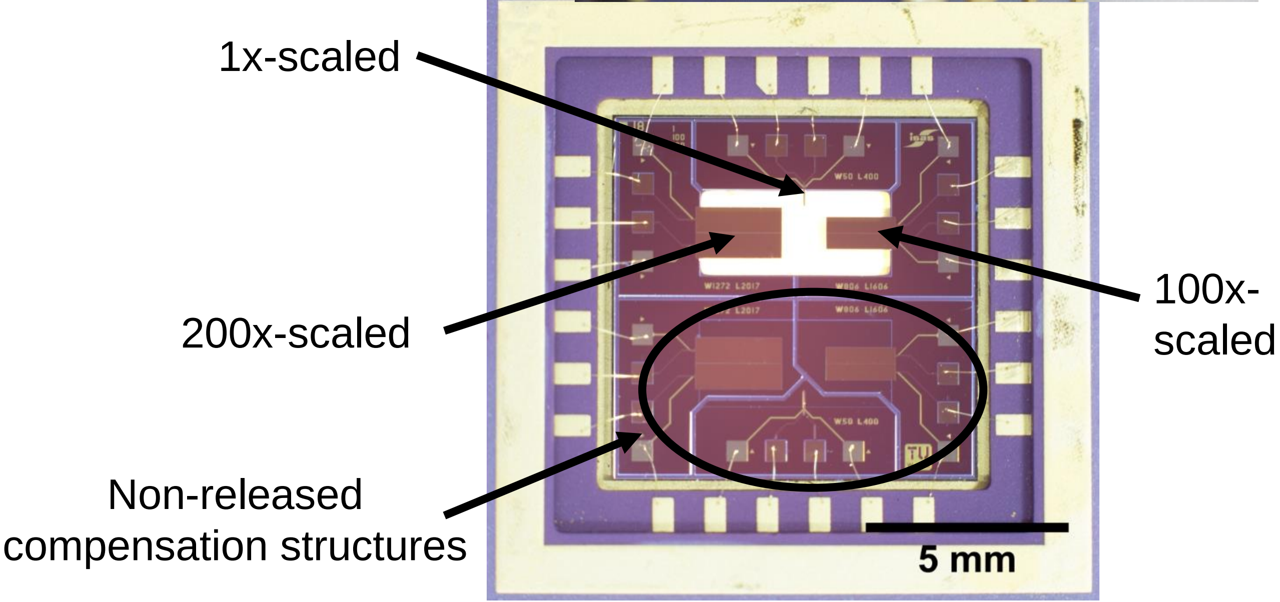

Study on the In-Plane Vibration Mode III

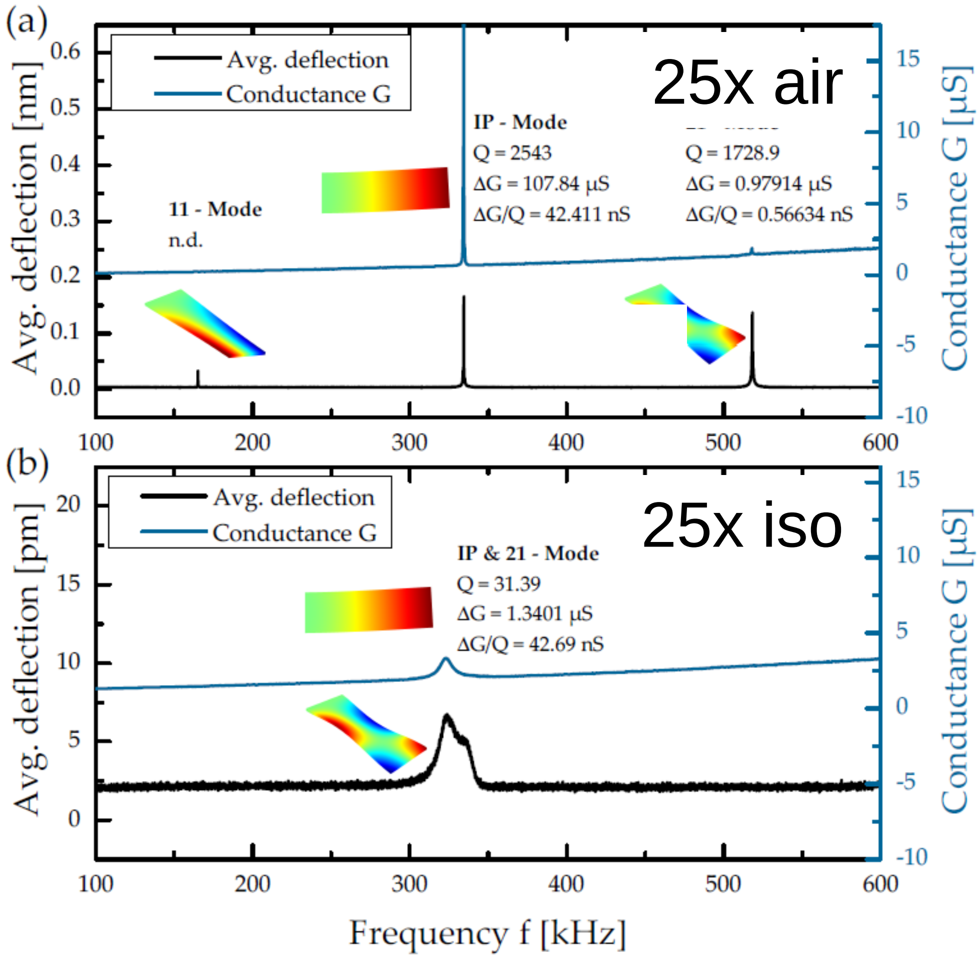

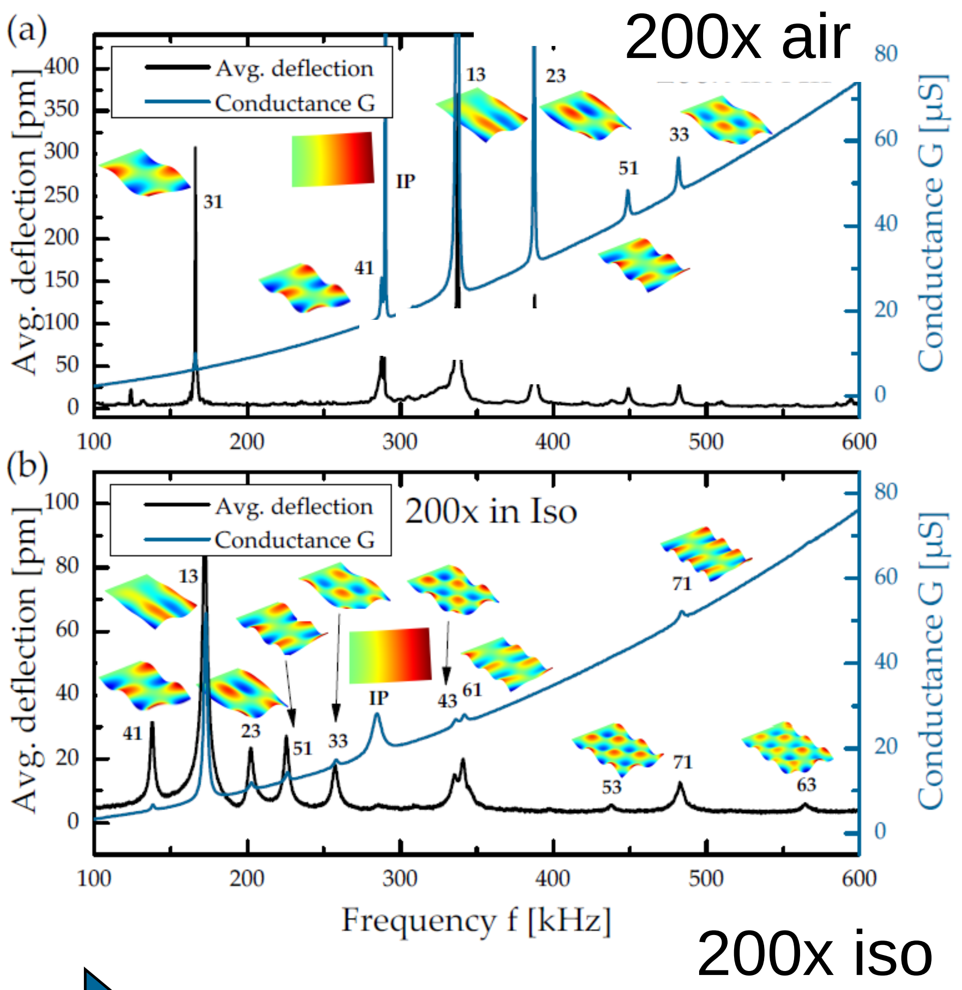

25x-scaled allows elec. measurement

200x-scaled: 13-mode!

M. Kucera et al., Sensors & Actuators B, Vol. 200, pp. 235-244, 2014, 2014.

Study on the In-Plane Vibration Mode IV

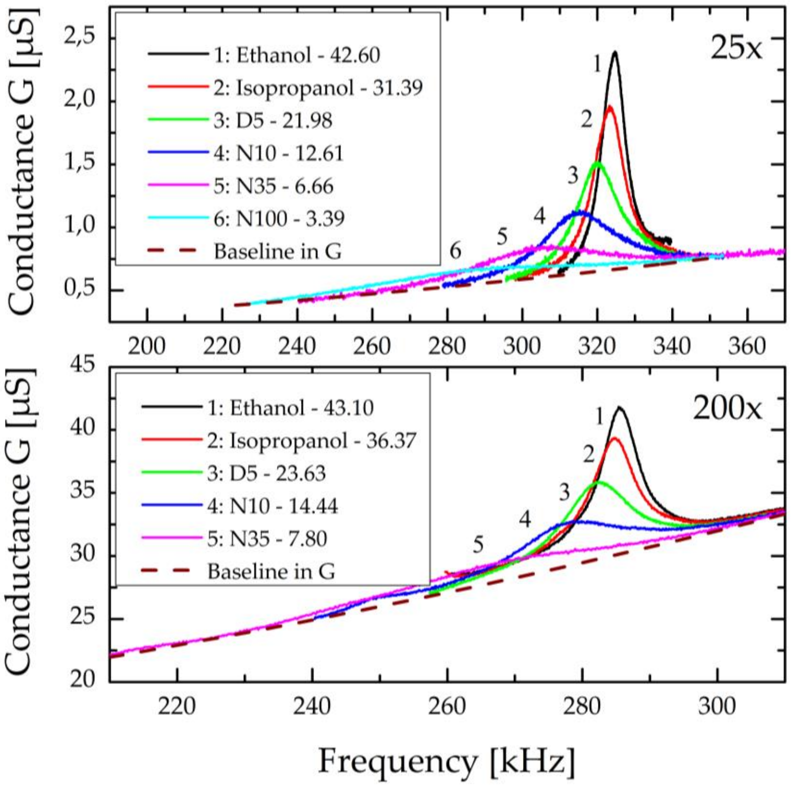

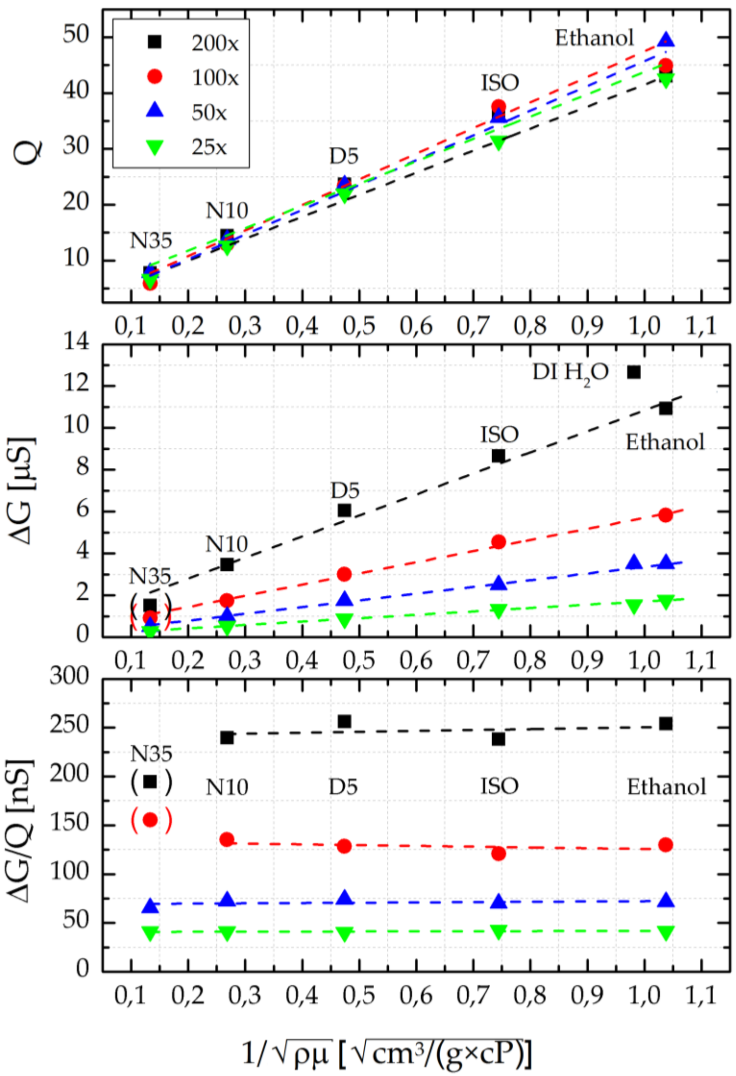

- Estimation of the conductance peak
- ΔG/Q ratio
  - Mode shape related
  - Electrode design related
  - Material and geometry related
  - From fluid properties independent key parameter

$$\Delta G = \frac{1}{R_\mathrm{m}} = \frac{{d_{31}}^2{\sigma_1}^2}{s_{11}^\mathrm{E}}\sqrt{\frac{3}{\rho_\mathrm{Si}\mathcal{E}_\mathrm{Si}}}\mathcal{E}_\mathrm{AlN}\frac{W^2}{TL}Q.$$

Study on the Multi Roof Tile-Shaped Vibration Mode

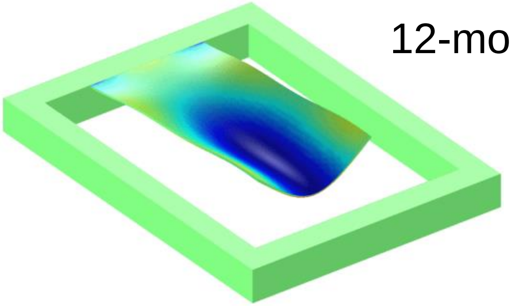
12-mode

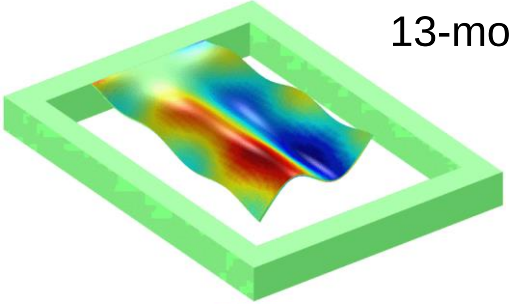
13-mode

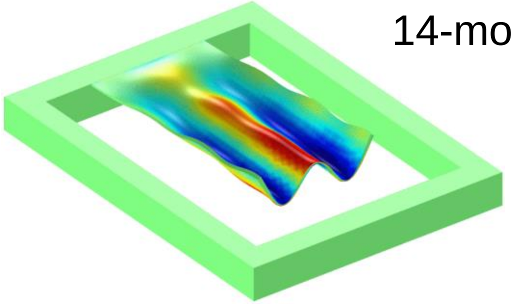
14-mode

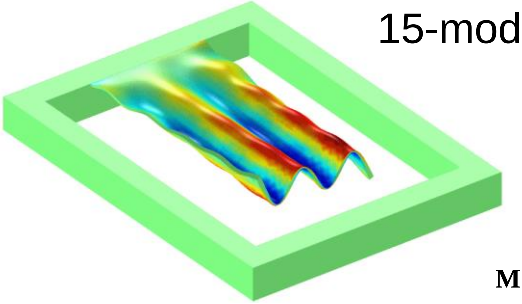
15-mode

- New class of vibration modes
- Evolution of the *Q*-factor in DI-water

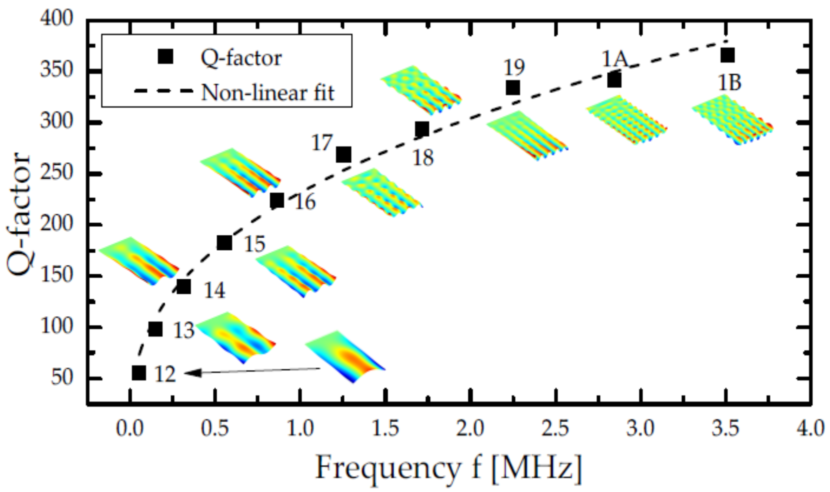

Order	Mode	f_{res} (kHz)	Q	ΔG (μS)	ΔG/Q (μS)
1	12	53,49	55,2	6,95	0,13
2	13	152,43	98,1	77,61	0,79
3	14	317,3	139,8	54,94	0,39
4	15	555,93	182,7	9,45	0,05
5	16	866,53	224	101,6	0,45
6	17	1256,64	268,3	328,37	1,22
7	18	1714,17	293,3	158,48	0,54
8	19	2250,98	333,9	24,81	0,07
9	1A	2842,84	341,4	149,67	0,44
10	1B	3508,69	366,2	443,37	1,21

M. Kucera et al., Applied Physics Letters, Vol. 104, pp. 233501, 2014.

Different roof tile-shaped modes in water

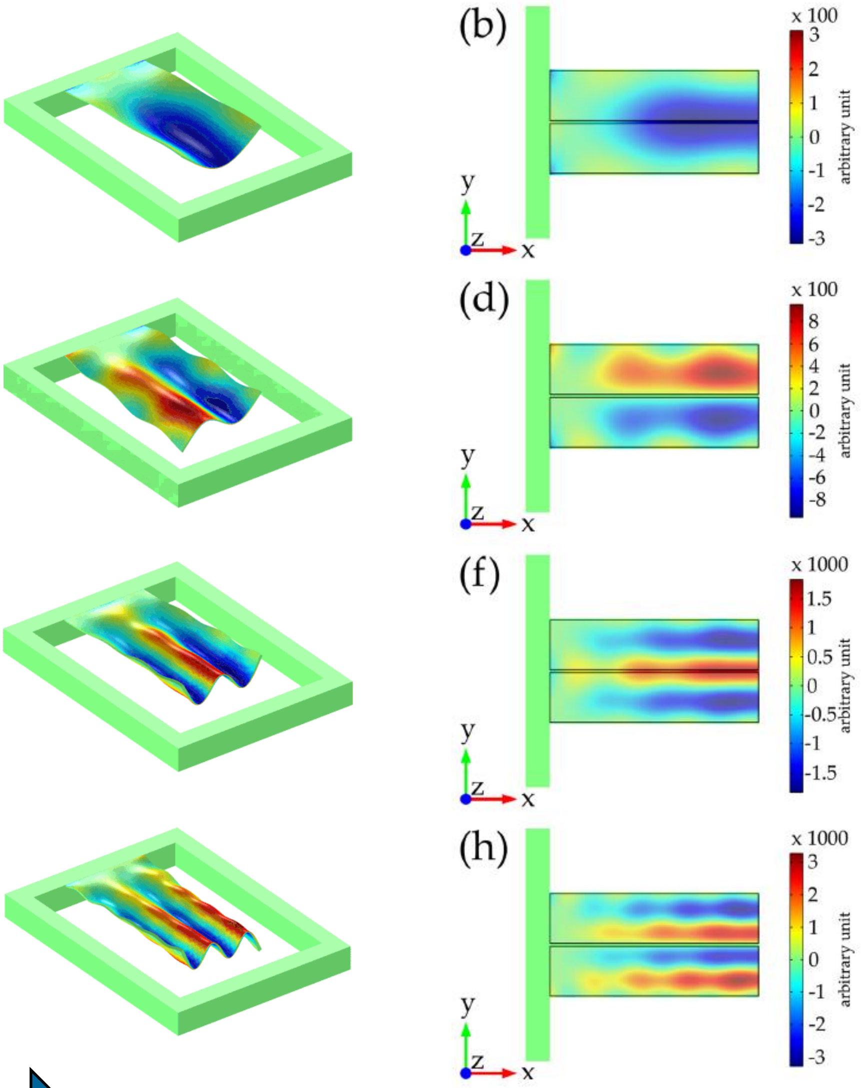

Order	Mode	f_{res} (kHz)	Q	ΔG (µS)	ΔG/Q (µS)
1	12	53,49	55,2	6,95	0,13
2	13	152,43	98,1	77,61	0,79
3	14	317,3	139,8	54,94	0,39
4	15	555,93	182,7	9,45	**0,05**

- Electrode shape must reflect the locally strained areas
- Electrode shape will be mode specific (to a certain degree)

Optimization of electrode design → large increase in measurement signal

Kucera, M., et al., Applied Physics Letters 107 (2015) 053506.

Optimized vs. non-optimized electrode design

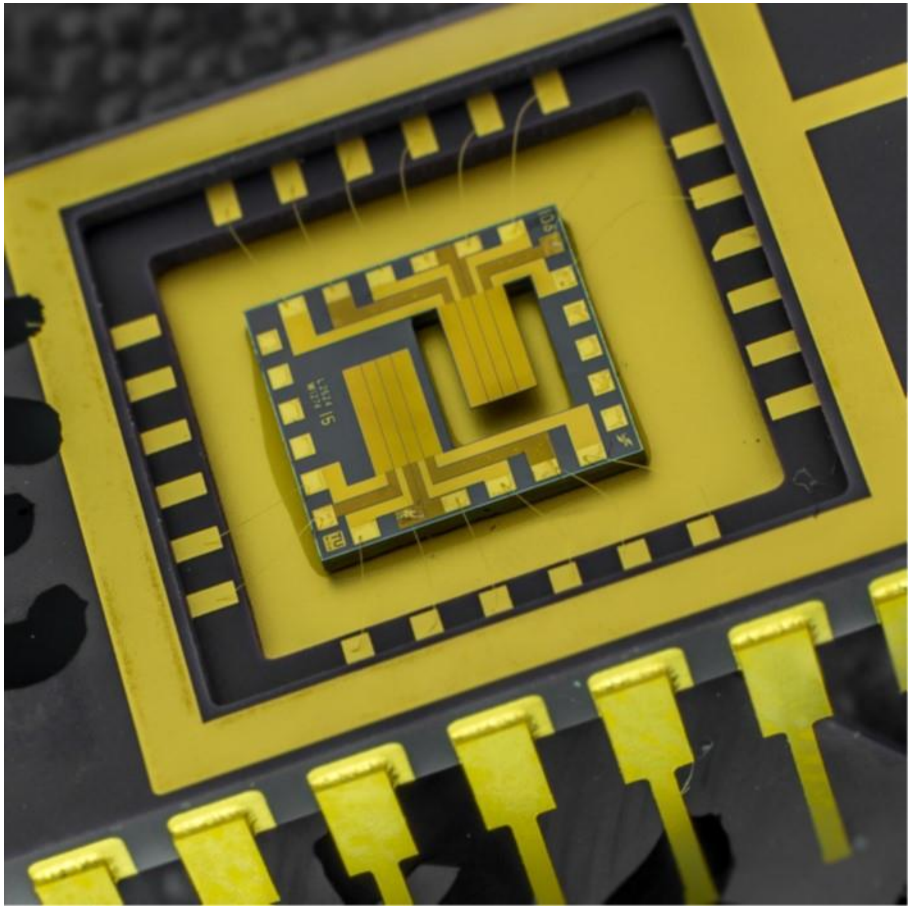

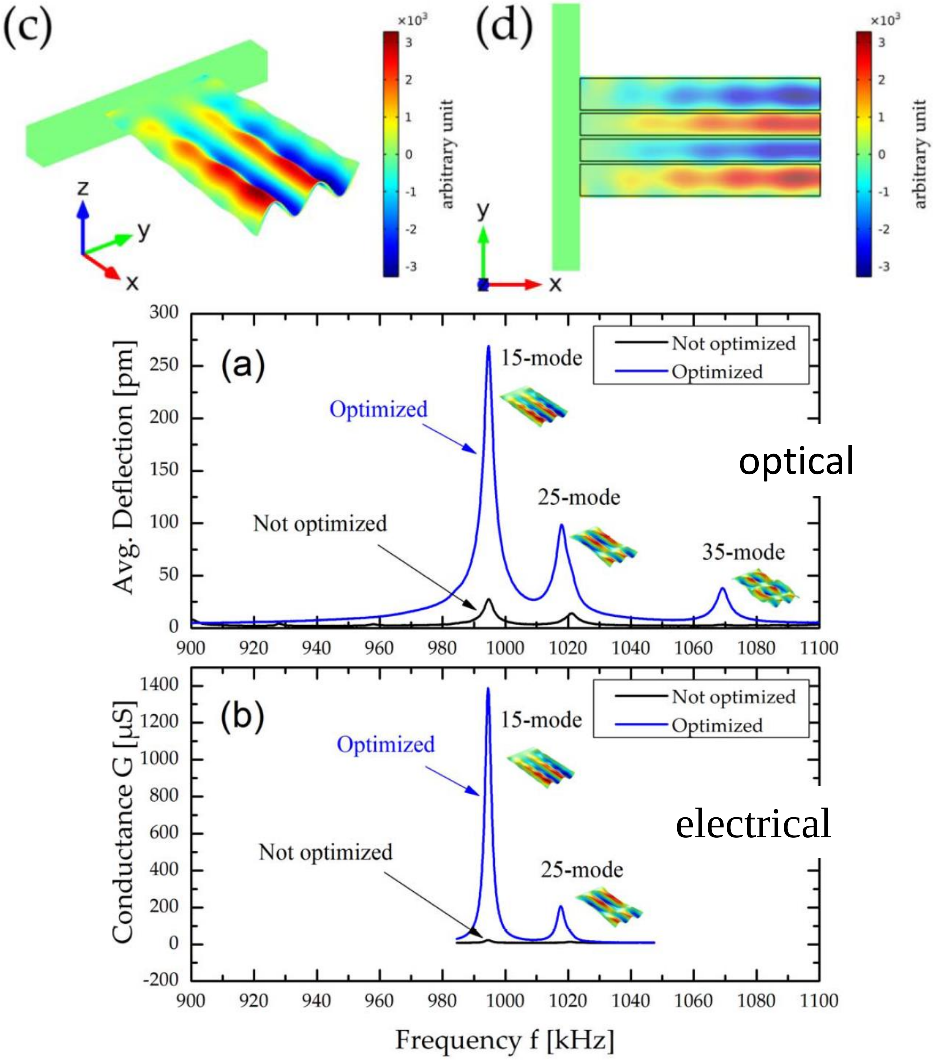

optical

electrical

10 × higher deflection
100 × higher conductance peak

Pfusterschmied, G., et al., Proceedings of the IEEE International Conference on Micro Electro Mechanical Systems (MEMS), 2015.

Roof tile-shaped mode at different temperatures

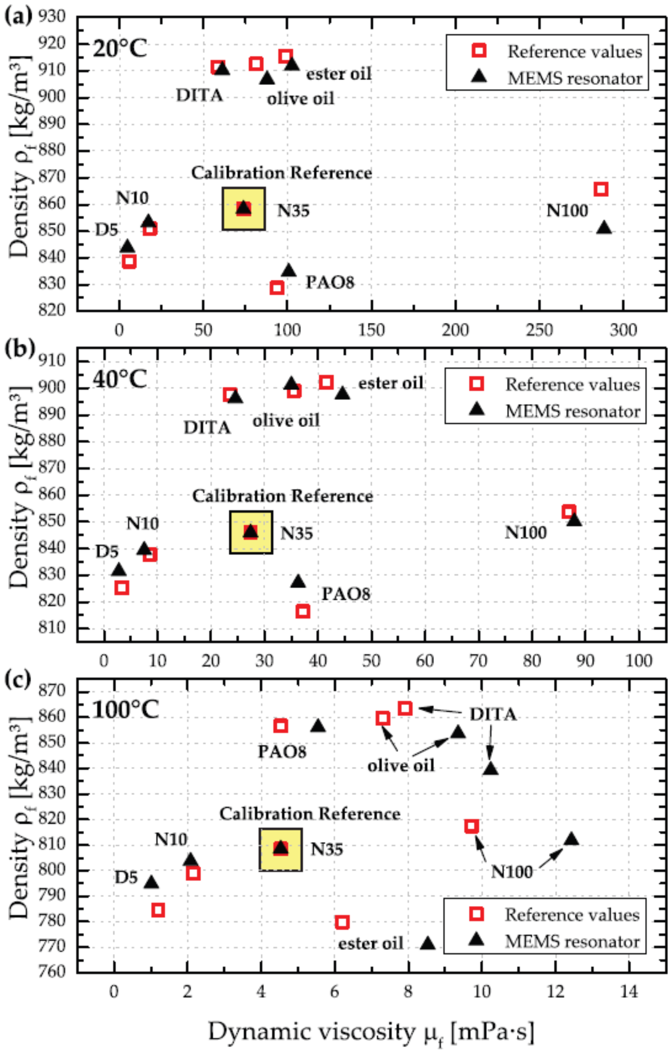

- Small deviation for density (averaged 0.76% at 20 °C, 0.55% at 40 °C, 1.04% at 100 °C)
- Deviation much larger for viscosity (6.35% at 20 °C, 6.87% at 40 °C and 23.44% at 100 °C)
- Possible solution

  → higher order modes with optimized electrode designs

  → Better calibration method

Good accuracy for density, low accuracy for viscosity measurements

Pfusterschmied, G., et al., Journal of Micromechanics and Microengineering, Vol. 25, pp. 105014 (8pp), 2015.

Vibrational Energy Harvesters – Evaluation of AlN and ScAlN I

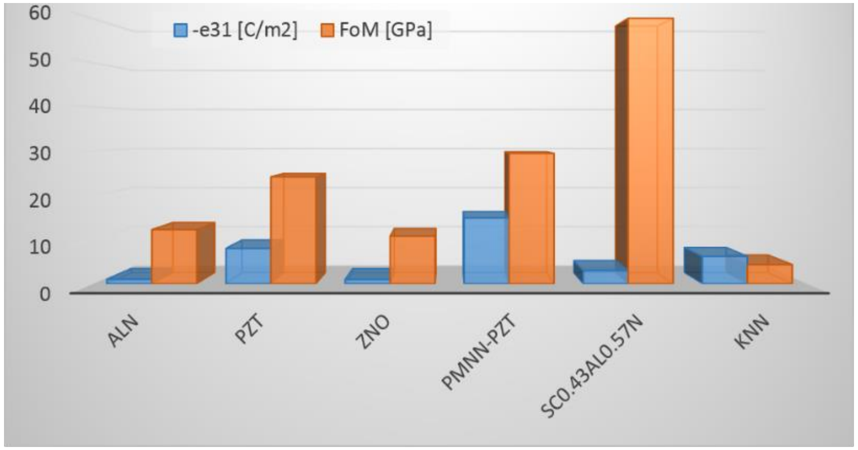

$$P_{EH} \propto FOM = \frac{e_{31}^2}{\varepsilon_0 \varepsilon_r} \qquad P_{EH} \propto FOM \approx \frac{d_{31}^2}{\varepsilon_0 \varepsilon_r Y_1^2}$$

Evaluation

- Maximum power output
- Variation of load resistance R_L
- Frequency sweep at first Eigenmode

Measurement Set-up

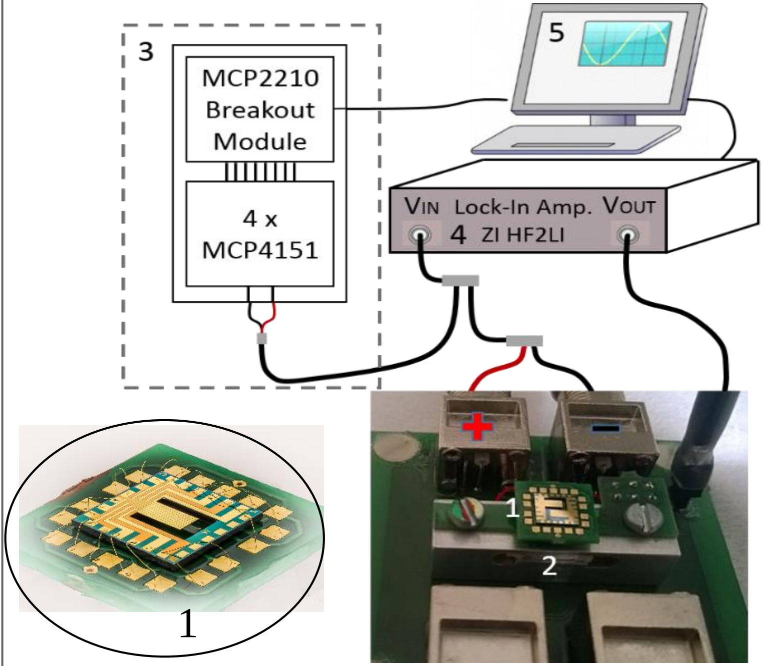

1: Cantilever & PCB
2: Shaker
3: Steckbrett mit 4x digitalen Potentiometer (max. 400 kΩ) & USB Controller
4: Zürich Instruments Lock-In Verstärker
5: PC mit LabView Implementierung.

Vibrational Energy Harvesters – Evaluation of AlN and ScAlN II

P … max. power vs. load

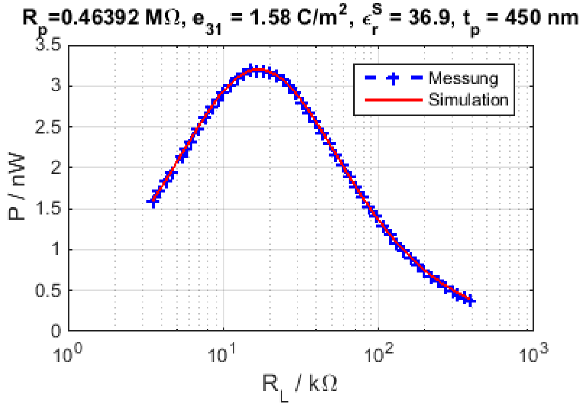

Q … quality factor

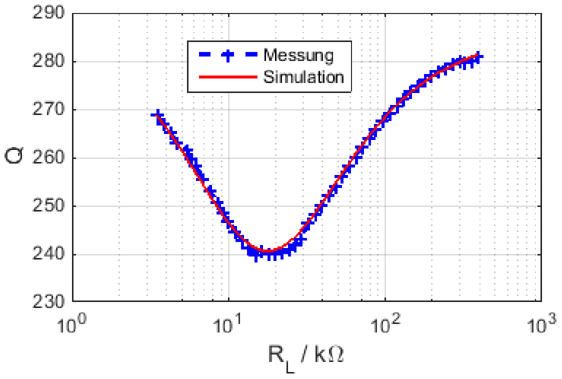

f_{res} … resonance frequency

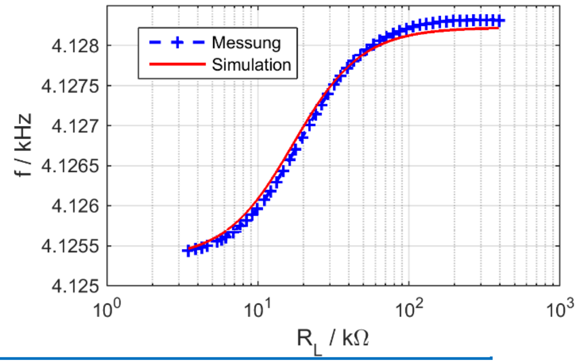

Piezoelectric coefficients

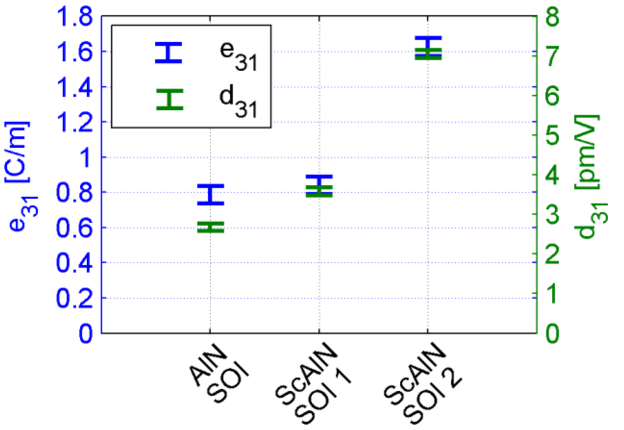

Maximum output power

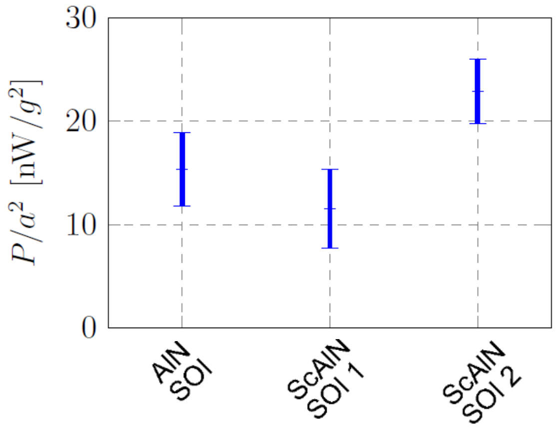

- Effective e_{31} is increased by ~200%, similar to d_{31}
- Maximal output power is doubled

ScAlN leads to increased power output compared to AlN

Mayrhofer, et al., ScAlN MEMS Cantilevers for Vibrational Energy Harvesting Purposes, **Journal of Microelectromechanical Systems, Vol. 26, No.1, 102-112, 2017.**

Research topic:

Energy Harvesting for Wireless Sensor Nodes

Why Energy Harvesting at Aircrafts?

[1]

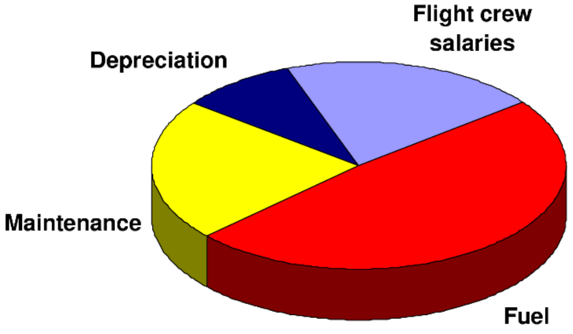

[3]

[1] www.tagesschau.de, aufgerufen am 25. 9. 2011
[2] ICAO Data. Airline Financial Detail Report. Technical report.

Thermoelectricity & Fundamental Module Concept

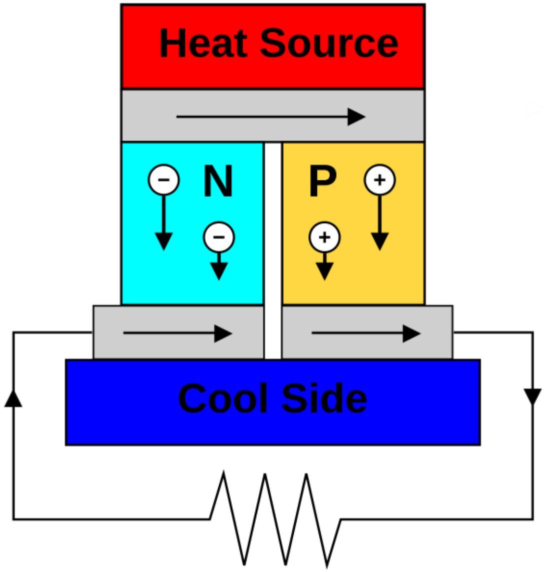

$$U = S_{AB} \cdot \Delta T$$

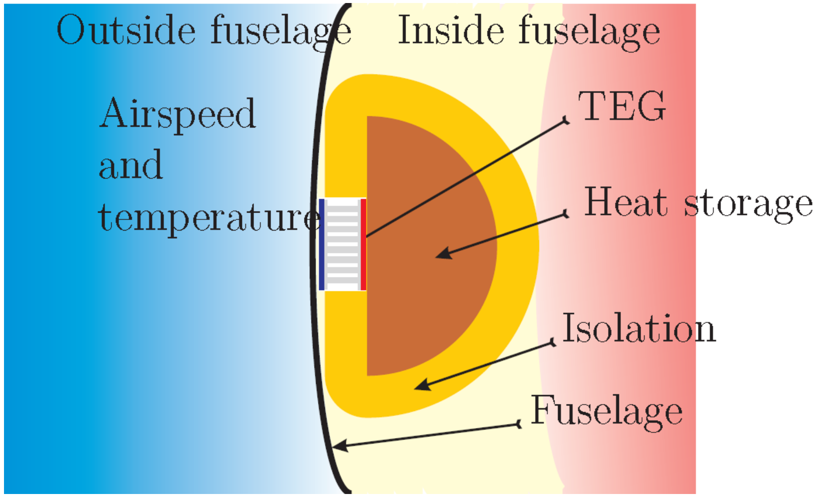

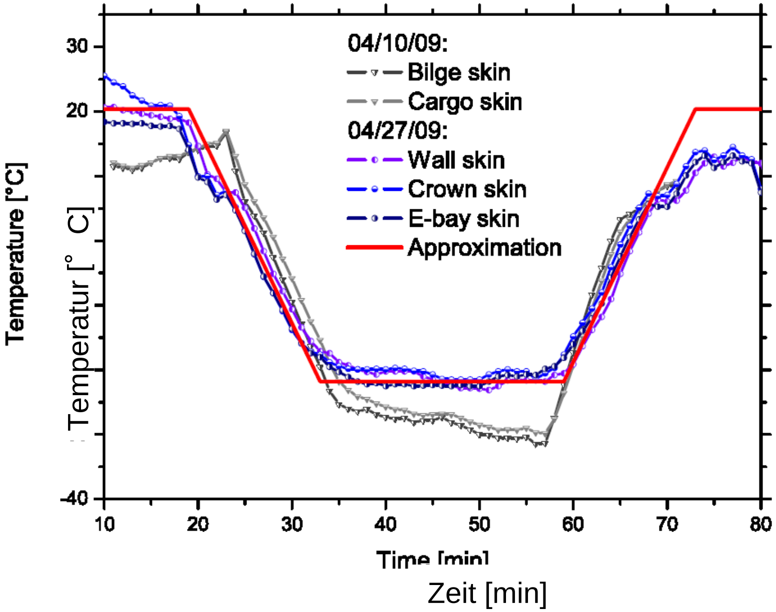

Dynamic Energy Harvesting:

Ground - Fuselage temperature: 20°C

Cruising - Fuselage temperature: -20°C (and even lower)

- Temporally restricted energy generation

+ easy to install

D. Samson et al., Journal of Electronic Materials, Vol. 39, No. 9, pp. 2092-2095, 2010.

Energy Harvesting for SHM I

COMSOL FEM simulations based on heat conduction equation to evaluate design aspects and to determine the energy output

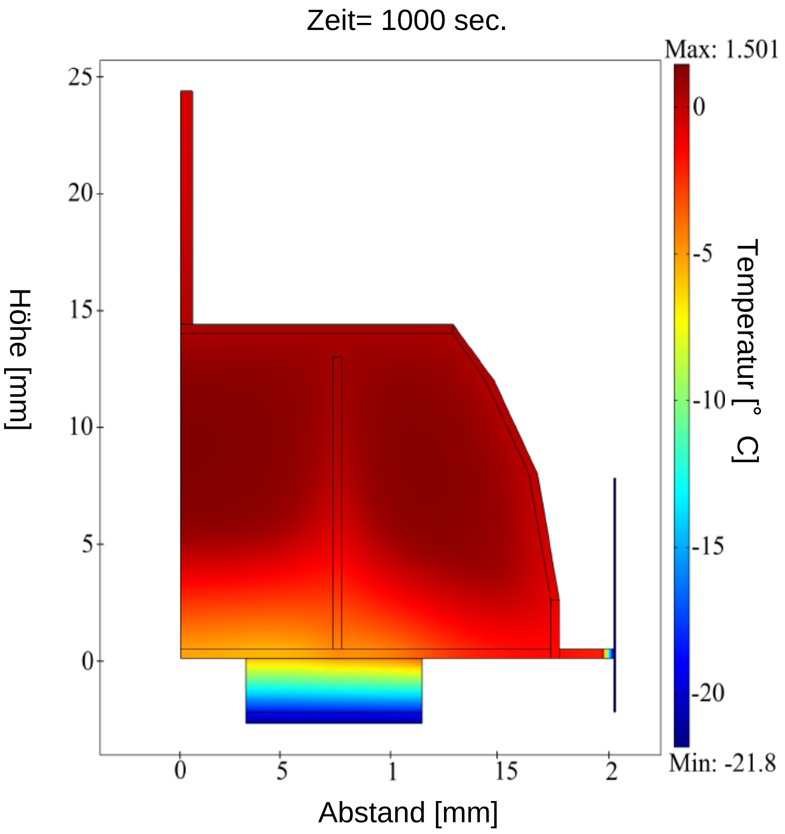

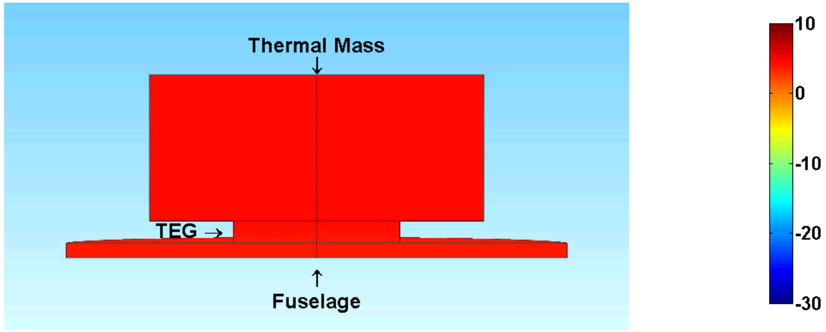

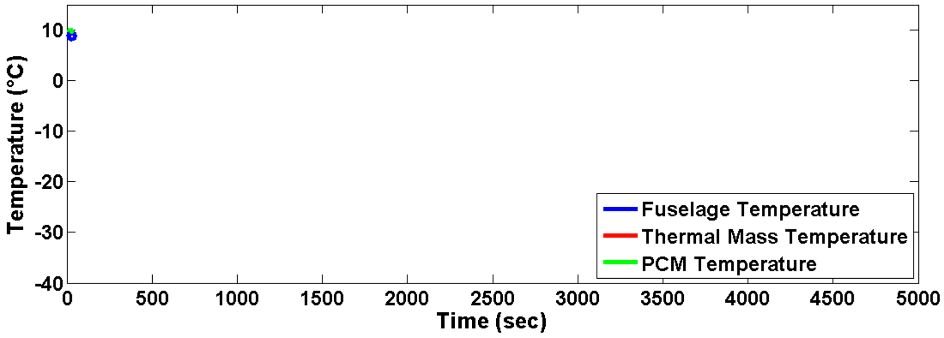

D. Samson et al., Sensors & Actuators A, Vol. 172, pp. 240-244, 2011.

Energy Harvesting for SHM II

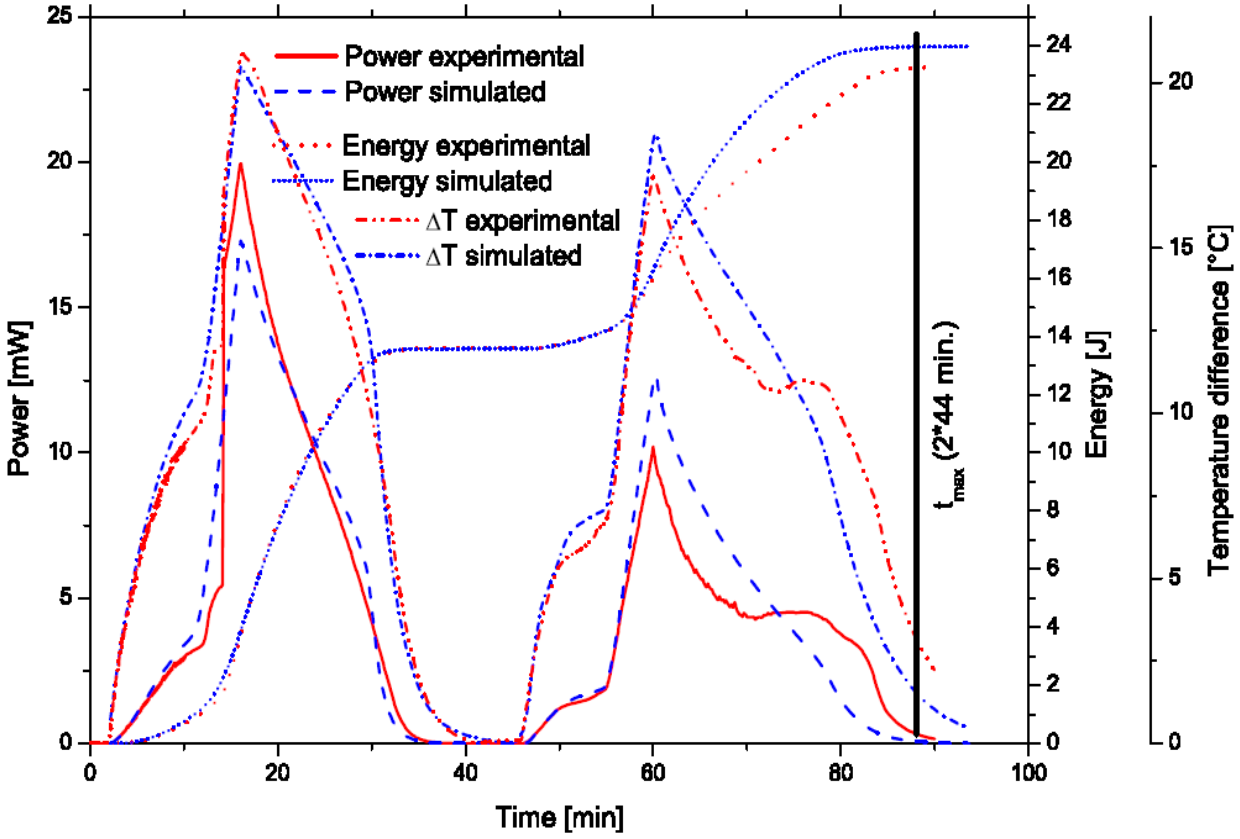

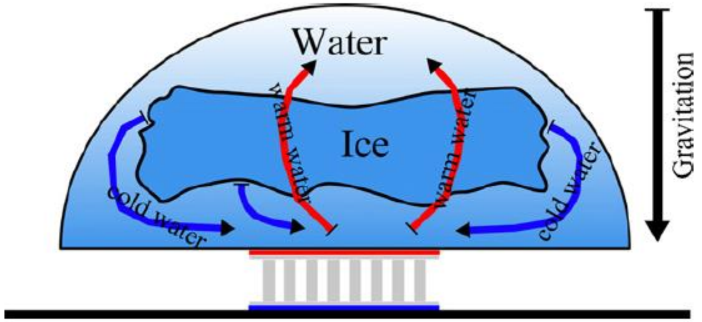

Energy output with 10g H_2O ~ 6.5 mWh

Energy Harvesting for SHM III

Test flight with DLR A320 D-ATRA:

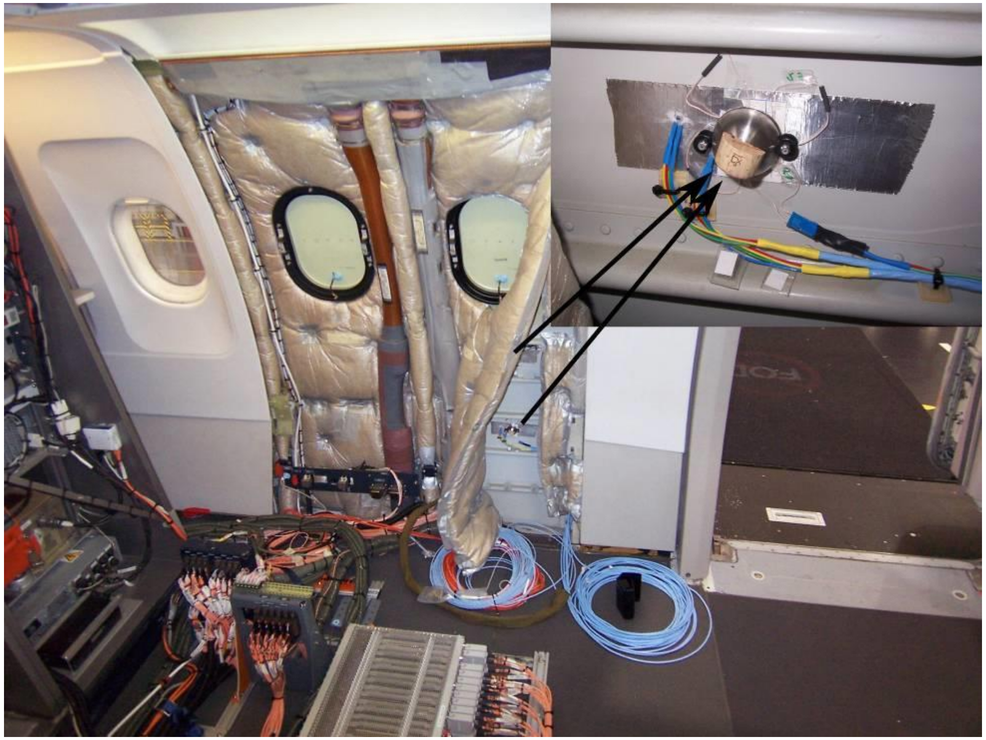

A. Elefsiniotis, et al., Journal of Electronic Materials, Vol. 42, Iss. 7, pp. 2301-2305, 2013.

Energy Harvesting for SHM IV

- Highest Altitude >30,000ft.
- Difference on outside and fuselage temperature due to aerodynamic heating
- Most energy is harvested during take-off!
- Power peak @~17mW
- Energy Harvested:

✓EH Device#1: ~22J

✓EH Device#2: ~24J

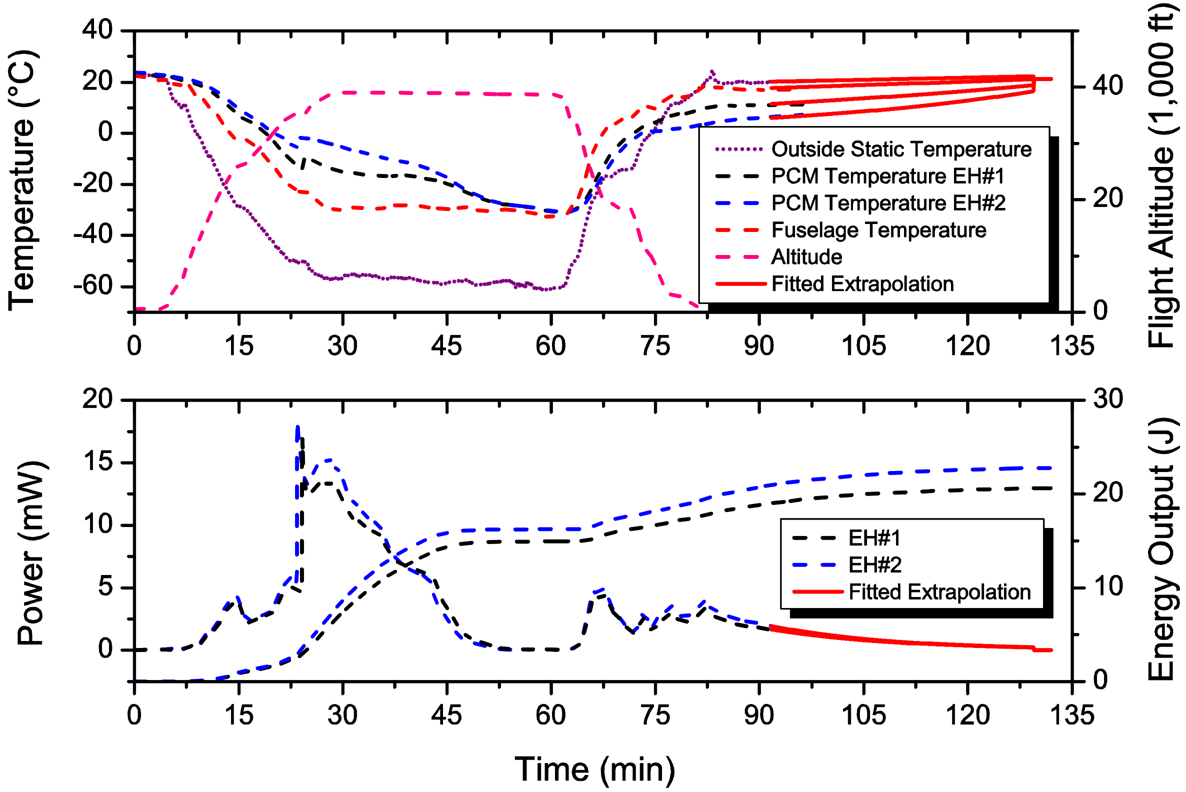

A. Elefsiniotis, et al., Journal of Electronic Materials, Vol. 42, Iss. 7, pp. 2301-2305, 2013.

Thank you
for your attention!

Questions?